A nonlinear tunable piezoelectric resonant shunt using a bilinear component: theory and experiment

Zein Alabidin Shami (zein_alabidin.shami@ensam.eu)
Arts et Metiers ParisTech - Centre de Lille https://orcid.org/0000-0002-5470-4957
Olivier Thomas
Arts et Metiers ParisTech - Centre de Lille
Christophe Giraud-Audine
Arts et Metiers ParisTech - Centre de Lille

Research Article

Keywords: Piezoelectric shunt absorber, Nonsmooth component, bilinear absorber, 2:1 internal resonance, Nonlinear Oscillations, Diode

Posted Date: September 23rd, 2022

DOI: https://doi.org/10.21203/rs.3.rs-2069664/v1

A nonlinear tunable piezoelectric resonant shunt using a bilinear component: theory and experiment

Zein A. Shami · Christophe Giraud-Audine · Olivier Thomas

Received: date / Accepted: date

Abstract In this article, we propose a new concept for tuning a resonant piezoelectric shunt absorber thanks to the use of a nonsmooth electronic component. It consists in adding in the resonant shunt circuit a voltage source which is a bilinear function of the voltage across the piezoelectric patch. The main advantage is the ability to change the electrical resonance frequency with the bilinear component gain, enabling a tuning as well as a possible reduction of the required inductance value. Because of the intrinsic nonlinear nature of the bilinear component, a multi-harmonic response is at hand, leading to a nonlinear coupling between the mechanical and electrical modes. Two particular tunings between the electrical and the mechanical resonance frequencies are tested. The first one is one-to-one, for which the electrical resonance is tuned close to the mechanical one. It is proved to be similar to a classical linear resonant shunt, with the additional tuning ability. The second case consists in tuning the electrical circuit at half the mechanical resonance, leading to a two-to-one (2:1) internal resonance. The obtained response is also found to be similar to a classical resonant shunt near the main resonance. In either case, the shunt performances are analytically and numerically studied, leading to optimal values of the design parameters as well as an estimation of the amplitude reduction provided by the shunt. Finally, experimental validation is proposed, targeting the damping of the twisting mode of a hydrofoil structure, in which the bilinear component is realized with a diode.

Keywords Piezoelectric shunt absorber, Nonsmooth component, bilinear absorber, 2:1 internal resonance, Nonlinear Oscillations, Diode

1 Introduction

Piezoelectric shunt absorbers represent an efficient way to attenuate the vibrations of structures under external excitation, especially when the size and weight constraints are presented. Those absorbers were proposed in [1] as an extension to the mechanical absorbers by utilizing a piezoelectric (PE) transducer connected to a dedicated electronic circuit.

Z.A. Shami, O. Thomas
Arts et Métiers Institute of Technology, LISPEN, HESAM Université, F-59000 Lille, France
E-mail: zein_alabidin.shami@ensam.eu,olivier.thomas@ensam.eu

C. Giraud-Audine
Arts et Métiers Institute of Technology, L2EP, HESAM Université, F-59000 Lille, France
E-mail: christophe.giraud-audine@ensam.eu

The simplest architectures of those shunt circuits are the resistive shunt (R-shunt, including a simple resistor) and the resonant shunt (RL-shunt, composed of a resistor and an inductor L), which are passive absorbers with a linear behavior. While the R-shunt dissipates the energy in heat form, the RL-shunt consists in coupling an electrical resonator (an RLC circuit, with C being the intrinsic capacitance of PE patch) to the host structure. It is thus an electrical analogue of a tuned mass damper (TMD) which can be tuned in a similar manner to achieve an optimal attenuation. In this context, it has been shown through the optimal study of the RL-shunt in [2] that for a given mechanical damping ratio, the optimal attenuation depends only on the PE coupling factor. Thus, enhancing the absorber performance can be done by increasing the PE coupling using, for example, a negative capacitance [3] or by optimizing the placement of the PE patch on the host structure [4]. Two main issues are encountered with the PE shunts: i) their sensitivity to any change in the resonance frequency of the structure [5], ii) for some applications targeting low-frequency modes, a very high inductance is required, which can be a practical issue [6, 7]. In addition, the R and RL-shunts act near a single structure mode, but they can be extended for multi-modal attenuation through multiple attachments [8–10]. One can refer further to the following reviews [11, 12] for a wider illustration regarding the optimization and different applications of the PE shunts.

PE shunts properties can be enhanced by intentionally introducing a nonlinear component in the shunt circuit to exploit some purely nonlinear features. An example of such applications is the so-called nonlinear energy sink "NES", introduced in [13], and realized theoretically and experimentally with piezoelectric shunt methodology in [14] and [15], respectively, by adding cubic nonlinear component in the shunt circuit. Another example is the so-called nonlinear tuned vibration absorber "NLTVA" introduced in [16] and realized with PE shunt theoretically [17] and experimentally [18]. Recently, a new semi-passive absorber, introduced in [19] and realized experimentally in [20], exploited a two-to-one (2:1) internal resonance and a saturation phenomenon by adding a quadratic nonlinear component in a classical RL-shunt. This concept was improved to correct an unwanted detuning by adding a cubic component, as shown theoretically in [21] and experimentally in [22].

In many applications, the nonlinearities can be presented (or approximated) in a polynomial form (i.e., quadratic or/and cubic). In essence, polynomial nonlinearities naturally appear in a wide range of nonlinear models involving geometric and material nonlinearities such as thin beam and plate models [23, 24]. The free and forced response of systems involving such types of nonlinearities can be analyzed analytically (up to a certain order) using several methods such as perturbation techniques [25], elliptic functions [26], and normal form [27]. However, in some other applications involving clearance [28], vibro-impacts [29] or dry friction [30, 31], nonsmooth piece-wise functions naturally appear in the model, leading to strong nonlinear effects.

Utilizing nonsmooth nonlinear components for vibration reduction is firstly introduced in [32] to enhance the design of the NES to act as shock isolators. A lot of studies were then conducted to analyze the energy transfer between linear and nonsmooth NES attachments. For example, the targeted energy transfer between a single degree of freedom linear system and nonsmooth NES is studied in [33]. Also, the dynamics of a NES of non-polynomial piece-wise potential is investigated in [34]. In addition, introducing a nonsmooth component led to the design of vibro-impact NES where detailed design rules were given in [35]. A recent theoretical and experimental study [36] proposed an enhanced NES by using a cubic spring in addition to a piece-wise linear spring.

To the authors' knowledge, the only attempt to use a nonsmooth component in a PE shunt methodology involved the synchronized switch damping (SSD) technique. The latter idea is proposed in [37] for piezoelectric transduction that is switched between two distinct shunt impedances, in synchronicity with the oscillations of the host structure [38]. The principle is the following: when the system is moving away from equilibrium, a voltage is applied such that the piezoelectric force resulting tends to restore the system to its equilibrium point. Various topologies have been proposed regarding the circuit connected in series with the patch via the switch: a simple resistor [37], a resistor and an

inductor to increase the voltage inversion [39] or the same circuit with an added static voltage source [40, 41]. In the latter case, the voltage may have to be controlled as well to avoid instabilities [42]. This technique proved to be efficient in terms of vibration reduction, but it can become complicated to tune in practice due to the imperfection of synchronization time required [38] as well as to the creation of higher harmonics and noise [43].

The main originality of this work is to present the design of a tunable PE resonant shunt with a nonsmooth voltage component, without any required synchronization. In practice, the nonsmooth voltage component can be realized in a passive way with a half-wave rectifier circuit that includes a diode, so that the bilinear function of the voltage across the piezoelectric transducer is obtained. In addition, the proposed design of the nonsmooth component allows us to tune the resonance frequency of the shunt circuit without changing the inductance. Thus, a lower inductance can be set for the optimum design, which is an advantage when considering low-frequency modes. This paper focuses on the theoretical bases of the absorber and its experimental proof of concept, by targeting the mitigation of the first twisting resonance of a hydrofoil structure.

This paper is organized as follows: in section 2, the theoretical study is illustrated, showing the main governing equations with the nonsmooth term in addition to their approximation. We also show the optimal study for one-to-one and two-to-one tuning cases of the electric resonance frequency. The obtained optimal parameters, in addition to the optimal attenuation, are then numerically verified. In section. 4 we show the experimental proof of concept where the nonlinear shunt circuit and the measurement protocol are illustrated. In addition, we show the experimental frequency responses for both tuning cases to validate the theoretical estimations.

2 Theoretical Analysis

2.1 Governing Equations

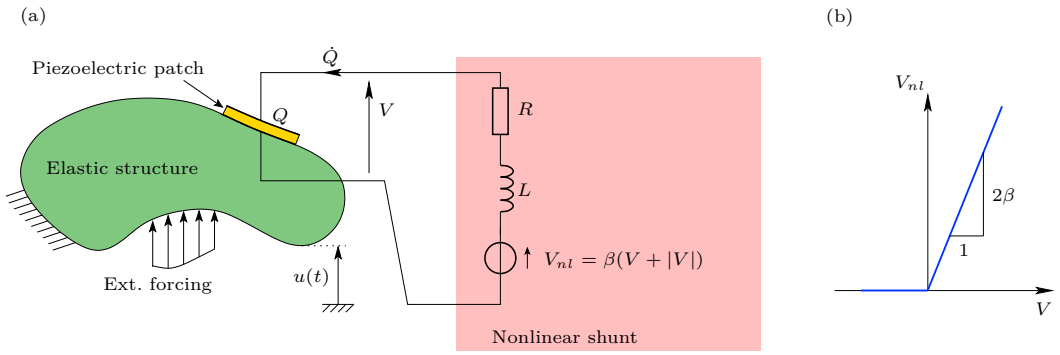

Fig. 1: (a) Elastic structure coupled to the nonlinear shunt circuit; (b) graph of the function $V \to V_{nl} = \beta(V + |V|)$.

We consider an arbitrary elastic structure subjected to an external excitation and connected to a shunt circuit via a piezoelectric patch, as shown in Fig. 1(a). Following [2, 19, 20], the displacement $u(\boldsymbol{x}, t)$ at position $\boldsymbol{x}$ in the structure and time t is truncated on one linear mode such that:

$$u(\boldsymbol{x}, t) = \psi(\boldsymbol{x})q(t), \tag{1}$$

where $\psi(\boldsymbol{x})$ is the mode shape and $q_i(t)$ is the i-th modal displacement. Then, $(Q(t),\, q(t))$ are the solutions of the following system:

$$\ddot{q}_i + 2\xi_i\hat{\omega}_i\dot{q}_i + \hat{\omega}_i^2 q_i + \frac{\theta_i}{m_i C_{\mathrm{p}i}} Q = \frac{F_i}{m_i}\cos\Omega t, \tag{2a}$$

$$\ddot{Q} + 2\xi_e\omega_e\dot{Q} + \omega_e^2 Q + \frac{\theta_i}{LC_{\mathrm{p}i}} q_i - \frac{V_{\mathrm{nl}}}{L} = 0. \tag{2b}$$

In the above equations, m_i, ξ_i, $\hat{\omega}_i$, θ_i, and F_i are, respectively, the modal mass, the mechanical damping ratio, the natural frequency in open circuit condition ($Q = 0$), the piezoelectric coupling coefficient, and the forcing, all corresponding to the i-th mode. $C_{\mathrm{p}i}$ is the effective capacitance of the piezoelectric patch for the i-th mode [3]. The electrical natural frequency ω_e and electric damping ratio ξ_e are defined as:

$$\omega_e = \frac{1}{\sqrt{LC_{\mathrm{p}i}}}, \quad \xi_e = \frac{R}{2}\sqrt{\frac{C_{\mathrm{p}i}}{L}}, \tag{3}$$

where R and L are the resistance and the inductance in the shunt circuit, respectively.

The PE patch voltage $V(t)$ can be defined as a function of $q_i(t)$ and $Q(t)$ using [2]:

$$V = \frac{1}{C_{pi}}(Q + \theta_i q_i). \tag{4}$$

We also define the dimensionless electromechanical modal coupling factor (EMMCF) of the i-th mode as:

$$k_i^2 = \frac{\hat{\omega}_i^2 - \breve{\omega}_i^2}{\hat{\omega}_i^2} = \frac{\theta_i^2}{\hat{\omega}_i^2 C_{\mathrm{p}i} m_i}, \tag{5}$$

with $\breve{\omega}_i$ the natural frequency in short circuit ($V = 0$).

In this study, we consider the nonlinear voltage component $V_{nl}(t)$ to be bilinear in terms of $V(t)$, as shown in Fig. 1(b), and expressed as:

$$V_{nl} = \beta(V + |V|), \tag{6}$$

where β is a dimensionless gain. The goal of introducing a nonsmooth nonlinearity in the form presented in Eq. (6) is first to generate even harmonics in the system, because it is not a symmetrical function of V, to possibly activate a 2:1 internal resonance, and second to use simple electrical components such as a diode or a transistor to practically realize it.

By substituting Eq. (6) in Eq. (2b) and eliminating V using Eq. (4), we obtain:

$$\ddot{q}_i + 2\xi_i\hat{\omega}_i\dot{q}_i + \hat{\omega}_i^2 q_i + \frac{\theta_i}{m_i C_{\mathrm{p}i}} Q = \frac{F_i}{m_i}\cos\Omega t, \tag{7a}$$

$$\ddot{Q} + 2\xi_e\omega_e\dot{Q} + \omega_e^2 Q + \omega_e^2\theta_i q_i - \beta\omega_e^2\left(Q + \theta_i q_i + |Q + \theta_i q_i|\right) = 0. \tag{7b}$$

Two important conclusions can then be drawn at this stage: (i) the governing equations in (7a,b) are indeed non-linear because of the non-smooth term ($|V| \implies |Q + \theta_i q_i|$) which only appears in Eq. (7b) and creates a harmonic distortion. (ii) although nonlinearities are present, (7a,b) *are in fact fully linear in amplitude*. For example, replacing F by $2F$ in Eq. (7a) leads to obtain $(2q_i,\, 2Q)$ instead of $(q_i,\, Q)$ (see also Fig. 10) since the absolute value function is linear in amplitude (i.e., $|2x| = 2|x|$ for $x \in \mathbb{R}$). However, it is not always additive or superposable, since $|x_1 + x_2| \neq |x_1| + |x_2|$ if $x_1 x_2 < 0$ for $x_1, x_2 \in \mathbb{R}$.

2.2 1DOF system with the nonsmooth term

To give a first analysis of the behavior of the coupled system (7a,b), we consider here only Eq. (7b), we exclude the piezoelectric coupling (i.e., setting $\theta_i = 0$), and we add a direct forcing term, leading to:

$$\ddot{Q} + 2\xi_e\omega_e\dot{Q} + \omega_e^2 Q - \beta\omega_e^2\left(Q + |Q|\right) = P\cos\Omega t, \tag{8}$$

where P is the forcing amplitude.

2.2.1 Free solution

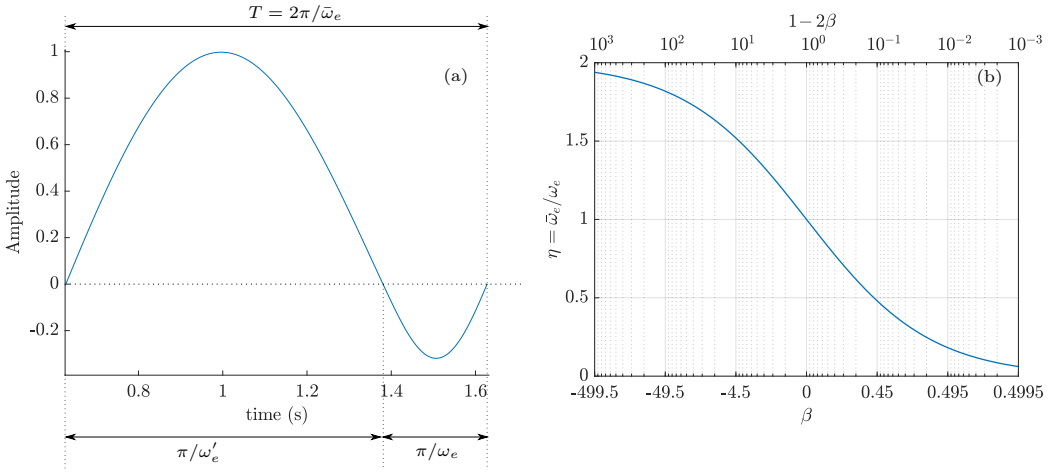

Fig. 2: (a) Example of the free response of Eq. (8) over one period. (b) Ratio $\eta = \bar{\omega}_e/\omega_e$ as a function of β.

To analyze the free response, we set $P = 0$, and we rewrite Eq. (8) as:

$$\ddot{Q} + 2\xi_e\omega_e\dot{Q} + \omega_e^2 Q = 0 \quad \text{if} \quad Q \leq 0, \tag{9a}$$

$$\ddot{Q} + 2\xi_e\omega_e\dot{Q} + \omega_e'^2 Q = 0 \quad \text{if} \quad Q \geq 0, \tag{9b}$$

where $\omega'_e = \omega_e\sqrt{1-2\beta}$. In the conservative case ($\xi_e = 0$), Eqs. (9) suggest that the free response is a succession of one half period of sine of period ω_e and one half period of sine of frequency ω'_e, as illustrated Fig. 2(a) . Then, the oscillation period can be expressed as:

$$T = \frac{2\pi}{\bar{\omega}_e} = \frac{\pi}{\omega_e} + \frac{\pi}{\omega'_e}, \tag{10}$$

where $\bar{\omega}_e$ is the modified angular frequency of the free response due to the nonsmooth term, which reads:

$$\bar{\omega}_e = \underbrace{\frac{2\sqrt{1-2\beta}}{1+\sqrt{1-2\beta}}}_{\eta}\omega_e = \frac{2\sqrt{1-2\beta}}{1+\sqrt{1-2\beta}}\frac{1}{\sqrt{LC_p}}, \qquad \eta = \frac{\bar{\omega}_e}{\omega_e}, \tag{11}$$

where η represents the ratio between the modified ($\bar{\omega}_e$) and unmodified (ω_e) natural frequencies. Eq. (11) proves that *even if the behaviour is nonlinear, the free oscillation frequency of Eq. (7b) does not depend on the amplitude*. Indeed, the oscillations are periodic but not harmonic since they are

the succession of two half sine functions of different periods: the more β is large, the more the two periods are different, and higher the harmonics content is expected.

Moreover, Eq. (11) suggests that given an electrical resonance frequency ω_e (i.e., given an inductance), the modified electrical oscillation frequency $\bar{\omega}_e$ can be adjusted according to the value of β. However, *the value of β should be less than 1/2* to avoid unstable response (if $\beta > 0.5$, ω_e' admits imaginary part). This feature is the main advantage of this nonlinear shunt circuit: by adjusting the nonlinear parameter β, one can tune the electrical circuit frequency at a particular value while fixing the inductance at a low value, which is an advantage for practical implementation. Fig. 2(b) shows the ratio η as a function of β, illustrating that it can be lowered to zero (at $\beta = 0.5$) and increased up to a factor of 2 (for $\beta \to -\infty$).

2.2.2 Forced Solution

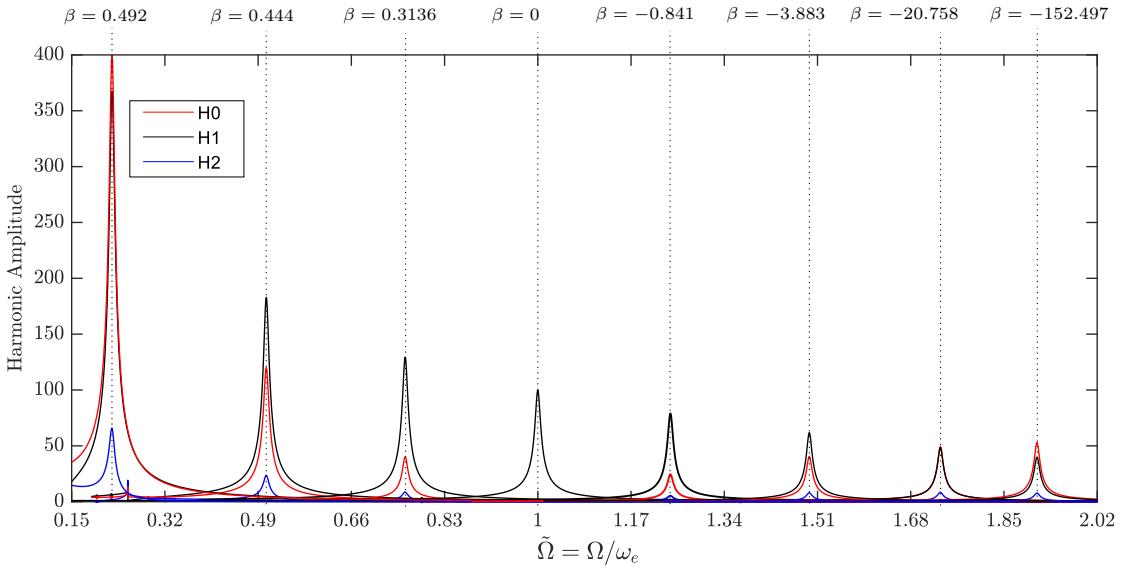

Fig. 3: Harmonics H0, H1 and H2 of the periodic solutions of Eq. (8) in the vicinity of the primary resonance, as a function of $\tilde{\Omega} = \Omega/\omega_e$ for $\xi_e = 0.005$. The harmonics' amplitude is normalized with respect to the excitation level. The vertical dotted black lines show the value $\bar{\omega}_e(\beta)$.

To analyze the forced response, we rewrite Eq. (8) in a dimensionless form by introducing the following parameters:

$$\tilde{t} = \omega_e t, \quad \tilde{Q} = Q\frac{\omega_e^2}{P}, \quad \tilde{\Omega} = \Omega/\omega_e. \tag{12}$$

Using the dimensionless parameters in Eq. (12), one obtains:

$$\ddot{\tilde{Q}} + 2\xi_e\dot{\tilde{Q}} + \tilde{Q} - \beta\left(\tilde{Q} + |\tilde{Q}|\right) = \cos\tilde{\Omega}\tilde{t}. \tag{13}$$

One can realize that the solution of Eq. (13) depends only on the damping ratio ξ_e and the gain β. As a consequence, *the shape of the resonance curve of Eq. (13) is independent of the excitation level* P and can be obtained for any value of P and ω_e using the scaling defined in (12).

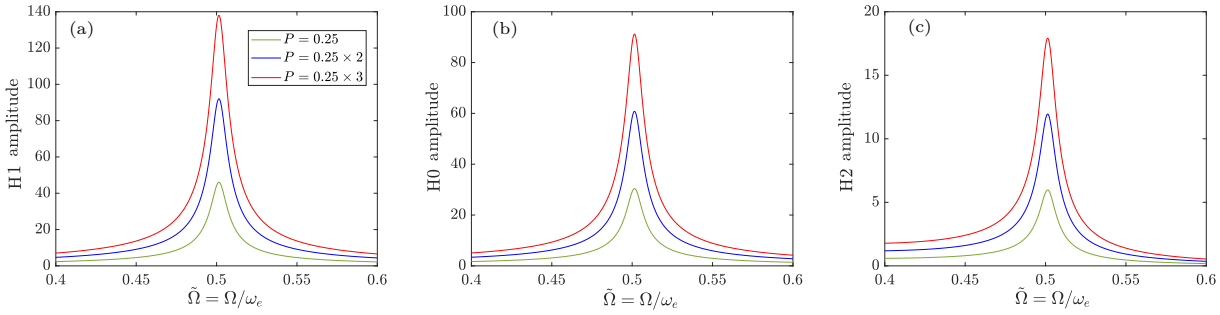

Fig. 4: Harmonics H1 (a), H0 (b) and H2 (c) of the periodic solutions of Eq. (8) in the vicinity of the primary resonance, as a function of $\tilde{\Omega} = \Omega/\omega_e$ for $\xi_e = 0.005$ and different excitation levels P. The numerical values used in the simulations are $\xi_e = 0.005$ and $\beta = 0.444$.

Eq. (13) is solved numerically with the continuation software MANLAB [44, 45] since there is no analytical solution at hand. MANLAB is based on a Harmonic Balance method to compute the periodic solutions. It requires a regularization of the nonsmooth term, which is discussed in Appendix B. Note that in all the numerical simulations with MANLAB, 40 harmonics were considered. Fig. 3 shows the dimensionless frequency response, normalized with respect to the excitation level, of the zeroth (H0), first (H1), and second (H2) harmonics of the periodic solutions of Eq. (8) for different values of β. Note that only H0, H1, and H2 harmonics are considered since they represent the dominant harmonics observed in the numerical simulations, and they will be relevant in the upcoming analysis. Indeed, other harmonics with lower amplitudes are present such as the third and fourth harmonics.

Two important conclusions can be drawn from the response shown in Fig.3. First, the nonlinear term creates a full harmonic content, with H0 being dominant in amplitude, H2 being significant but with lower amplitude, and the higher harmonics being negligible. Second, the relative amplitude of the harmonics with respect to the fundamental H1 increases with the absolute value of the nonlinear coefficient $|\beta|$: with $\beta = 0$, the response is fully linear with no harmonics, except H1. However, if β is close to 0.5 or tends to $-\infty$, the harmonic content increases significantly. Interestingly, the amplitude of H0 exceeds that of H1 for extreme values of β (e.g., for $\beta = 0.492$ and $\beta = -152.497$).

The most important observation is that the shape of each harmonic, considered separately, seems close to the frequency response of a linear oscillator near its resonance frequency, which is obtained here in the vicinity of the free oscillations frequency, for $\Omega = \bar{\omega}_e$. Such property is conserved even for higher excitation, as shown in Fig. 4, in which the linearity property with respect to the excitation level is clearly observed.

On the contrary to the quasi-linear behavior described above, the nonlinear nonsmooth term can generate a strongly nonlinear superharmonic response near $\Omega = \bar{\omega}_e/2$. This is emphasized in Fig. 5, which shows the superharmonic responses for different values of β, of the H0, H1, and H2 harmonics. The results suggest that the superharmonic response appears to be nonlinear (hardening effect with unstable branches), and the nonlinear effect increases with β. This suggests that introducing the nonsmooth term can represent an option for the application involving internal resonance (as will be discussed in section 3.2).

2.2.3 Forced response approximation with a linear oscillator

As discussed in the previous section, the nonlinear frequency response of the harmonics seems similar to the frequency response function (FRF) of a linear oscillator near the primary resonance. Thus, we

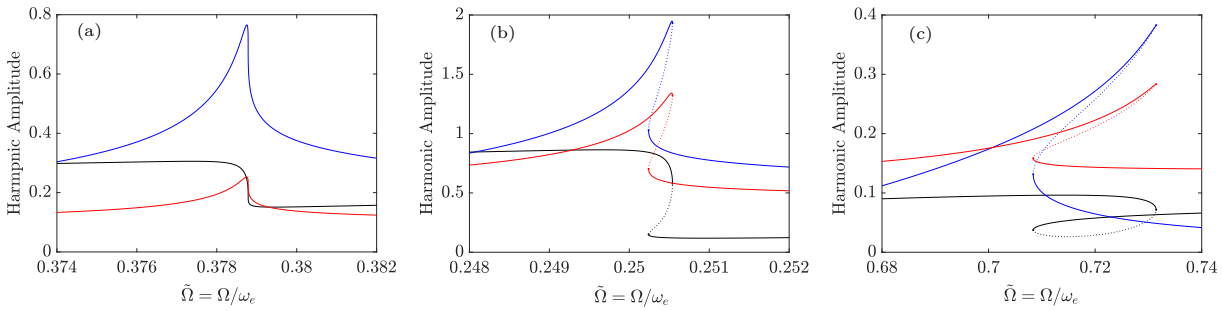

Fig. 5: Harmonics H0 (in red), H1 (in black), and H2 (in blue) of the periodic solutions of Eq. (8) in the vicinity of the superharmonic resonance of order two. (a) $\beta = 0.3136$, (b) $\beta = 0.444$, and (c) $\beta = -3.883$. The numerical values are $\xi_e = 0.005$ and $P = 0.1$. The solid and dotted lines denote the stable and unstable responses, respectively.

seek an approximation of Eq. (8) that is defined by the following linear oscillator, for $p = 0, 1, 2$:

$$\ddot{Q}_p + 2\bar{\xi}_e\bar{\omega}_e\dot{Q}_p + \bar{\omega}_e^2 Q_p = \phi_p P \cos \Omega t, \tag{14}$$

where Q_p is the approximated response of the p-th harmonic of $Q(t)$, $\bar{\xi}_e$ is the modified damping ratio due to the nonsmooth term, and ϕ_p is an unknown gain, corresponding to the p-th harmonic, introduced to quantify the difference between the analytical and numerical solutions and to be determined by fitting the analytical frequency response of Q_p with the numerical frequency response of the p-th harmonic. From a physical point of view, the gain ϕ_p enables quantifying the energy distribution at each harmonic due to the presence of the nonsmooth component.

To determine the modified damping ratio $\bar{\xi}_e$, we assume (and we will verify hereafter) that the nonsmooth term has no effect on the damping coefficient (i.e., the term multiplying $\dot{Q}$), and thus:

$$\bar{\xi}_e\bar{\omega}_e = \xi_e\omega_e \quad \Rightarrow \quad \bar{\xi}_e = \xi_e/\eta. \tag{15}$$

Then, the FRF of Q_p is expressed as:

$$Z_p(\Omega) = \frac{\mathring{Q}_p}{P} = \frac{\phi_p}{\bar{\omega}_e^2 - \Omega^2 + 2j\bar{\xi}_e\bar{\omega}_e\Omega}. \tag{16}$$

where $\mathring{Q}_p$ denotes the Fourier transform of $Q_p(t)$ and $j = \sqrt{-1}$. To validate the estimated damping ratio and to determine the gain ϕ_p, we set $\bar{\xi}_e$ according to Eq. (15) and we only vary the value of ϕ_p to fit the numerical FRFs, shown in Fig. 3, for each harmonic with their equivalent analytical ones, defined in Eq. (16). Examples of those fittings for different values of β are shown in Fig. 6 near the primary resonance. Notice the appearance of superharmonic responses, clearly observed in the H2 response in Fig. 6(c), not taken into account in our equivalent linear model.

Considering this numerical fitting, we can draw two conclusions. The first one is that the equivalent damping ratio $\bar{\xi}_e$, defined in Eq. (15), is the perfect one since the fitted equivalent linear FRFs match exactly the shape of the numerical (nonlinear) ones, by varying only the value of $\phi_{H\mathrm{p}}$ to reach the perfect fit.

The second conclusion is that by fitting the analytical and numerical frequency responses for H0, H1, and H2 for different values of β, the gain ϕ_p for each of those harmonics can be estimated as a function of β (it is shown by markers in Fig. 7). Note that the estimated values of ϕ_p are firstly plotted with respect to $\log_{10}(1-2\beta)$ and then mapped to the values of β. Additionally, the results prove that increasing $|\beta|$ leads to more distribution of energy to the other harmonics as both ϕ_0 and ϕ_2 increase.

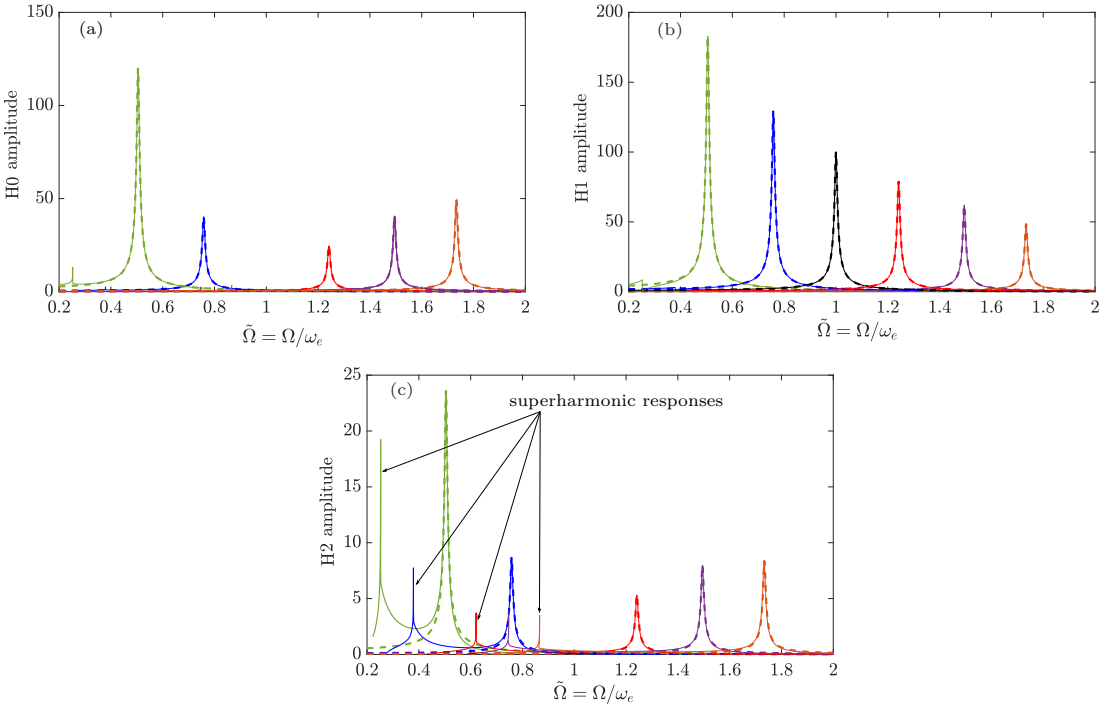

Fig. 6: Examples of the fitting between the numerical and analytical frequency responses, normalized with respect to the excitation level, of the harmonics H0 (a), H1 (b), and H2 (c). The numerical results, estimated by solving Eq. (13) with MANLAB, are depicted in solid lines and the analytical results, according to Eq. (16), are depicted in dashed lines. The fittings are performed near the primary resonance for $\beta \in \{0.444, 0.313, 0, -0.841, -20.758\}$ and $\xi_e = 0.005$.

Compatible with the results in Fig. 3, H2 harmonic has a lower influence compared to H0 even for high values of $|\beta|$. More precisely, it appeared that the amplitude of H2 tends to a constant value as $|\beta|$ increases. On the contrary, H0 harmonic admits larger influence in which ϕ_0 suggests higher value compared to ϕ_1 for extreme values of $|\beta|$.

Table 1: Polynomial coefficients a_m of $\phi_p(\beta)$ for $\beta > 0$.

	a_0	a_1	a_2	a_3	a_4	a_5	a_6
ϕ_1	1	0.0065	−0.1432	0.0610	−0.0078	0	0
ϕ_0	0	0.7354	0.002	−0.1528	0.0547	−0.0061	0
ϕ_2	0	0.1628	0.0066	−0.0825	0.0455	−0.0102	0.0008

Interestingly, those last results suggest that ϕ_p *admits a symmetric behavior with respect to* $\log_{10}(1-2\beta)$. Thus, to obtain a closed-form approximation of ϕ_p, which will be used in the further analysis, we seek a polynomial expression of ϕ_p as:

$$\phi_p(y) = \sum_{m=0}^{N} a_m y^m, \qquad y(\beta) = -\log_{10}(1-2\beta) = -2\log_{10}\left(\frac{\eta}{2-\eta}\right), \tag{17}$$

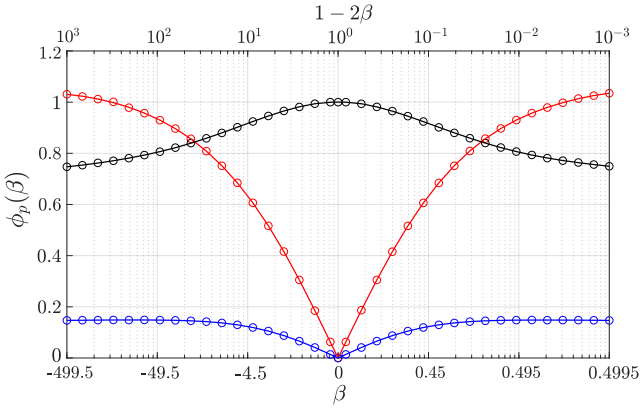

Fig. 7: ϕ_p as a function of β corresponding to harmonics H0 (red), H1 (black), and H2 (blue). The circles denote the values estimated by fitting the analytical and the numerical responses for each value of β, and the solid lines denote the closed form approximated polynomial curves.

where $N \in \mathbb{N}$ is the polynomial order and $a_m \in \mathbb{R}$ are the polynomial coefficients. Thanks to the symmetric property, the relation $\phi_p(y) = -\phi_p(y)$ can be used to estimate the coefficients a_m only for $y > 0$ (i.e., $\beta > 0$) and then directly obtain the coefficients for $y < 0$ (i.e., $\beta < 0$) by changing the sign of the coefficients a_m of the odd monomials (i.e. a_m with m odd). In addition, to take into account the fact that only H1 will respond for $y = 1$ (i.e., $\beta = 0$), we enforce constraints on a_0 for each harmonic such that $a_0 = 1$ for H1 and $a_0 = 0$ for H0 and H2. With the constraint enforcement on a_0, a good fitting between the polynomial expressions (solid lines in Fig. 7) and the obtained data (circle markers) required $N = 4$ for ϕ_1, $N = 5$ for ϕ_0, and $N = 6$ for ϕ_2. The estimated coefficients a_m for each harmonic are gathered in Table. 1 only for $\beta > 0$.

3 Response of the full system according to the tuning of the nonsmooth component

In this section, we study the response of the full system (7a,b) with two particular tunings of the nonsmooth term. Based on the analysis in section 2.2, two main points can be emphasized. First, it was shown that each harmonic of the response of the electrical oscillator could be considered separately and approximated by an equivalent linear system. This suggests using the first harmonic as an oscillator that can be tuned on one resonance of the host mechanical system to act as an RL-shunt, with the additional interest of tuning it using the nonsmooth gain β. This is investigated in section 3.1, by tuning the electrical oscillator on the i-th vibration mode, such that $\bar{\omega}_e \simeq \hat{\omega}_i$. Secondly, a nonlinear behavior was observed with the appearance of H0 and H2 harmonics and of a 1:2 superharmonic response of the electrical oscillator. This behaviour is a characteristic of a non-symmetric nonlinearity (see the curve $V_{\text{nl}} = f(V)$ in Fig. 1(b)) and suggests to investigate a 2:1 internal resonance, by tuning the electric oscillator at half the mechanical frequency ($\bar{\omega}_e \simeq \hat{\omega}_i/2$) and testing a transfer of energy from the mechanical oscillator to the electrical one, as already done using quadratic nonlinear terms in [19, 20, 22]. This is investigated in section 3.2.

3.1 One-to-one tuning of the nonlinear shunt ($\bar{\omega}_e = \hat{\omega}_i$)

3.1.1 FRF approximation

As analyzed in the previous sections, the nonlinear electrical oscillator (Eq. (7b)) oscillates with a fundamental harmonic (H1) that responds linearly around its primary resonance $\Omega \simeq \bar{\omega}_e$, suggesting that it can serve as a linear attachment similar to a standard RL-shunt. Thus, we consider here a tuning of β to have $\bar{\omega}_e = \hat{\omega}_i$: the modified electrical frequency is tuned to the open circuit natural frequency of the host structure, as a classical linear resonant shunt, expecting similar behavior.

For this tuning case, we are interested in the first harmonic response behavior. Then, we replace Eq. (7b) by its linear approximation (14). Since the external forcing is only applied on Eq. (7a), the PE coupling term $\theta/(LC_{\mathrm{pi}})q_i$ in Eq. (7b) is considered as a forcing term, thus a multiplication by ϕ_1 will be enforced based on the linear approximation in section 2.2.3. In addition, $\omega_e = 1/(\sqrt{LC_{\mathrm{pi}}})$ is replaced by the modified frequency $\bar{\omega}_e$. Thus, we arrive at the following approximation:

$$\ddot{q}_i + 2\xi_i\hat{\omega}_i\dot{q}_i + \hat{\omega}_i^2 q_i + \frac{\theta_i}{m_i C_{\mathrm{pi}}} Q = \frac{F_i}{m_i}\cos\Omega t, \tag{18a}$$

$$\ddot{Q} + 2\bar{\xi}_e\bar{\omega}_e\dot{Q} + \bar{\omega}_e^2 Q + \bar{\omega}_e^2\phi_1\theta_i q_i = 0. \tag{18b}$$

To simplify the writing of (18a,b), we define the following change of variables:

$$\tilde{t} = \hat{\omega}_i t, \quad \tilde{\Omega} = \frac{\Omega}{\hat{\omega}_i}, \quad \tilde{q}_i = \sqrt{m_i}q_i, \quad \tilde{Q} = \frac{1}{\bar{\omega}_e\sqrt{\phi_1 C_{pi}}}Q = \frac{\sqrt{L}}{\eta\sqrt{\phi_1}}Q, \quad f_i = \frac{F_i}{\hat{\omega}_i^2\sqrt{m_i}}, \tag{19}$$

where the dimensionless time $\tilde{t}$ and frequency $\tilde{\Omega}$ are different than those of section 2.2.2. The two following frequency ratios are also defined:

$$r_i = \frac{\omega_e}{\hat{\omega}_i}, \quad \bar{r}_i(\beta) = \frac{\bar{\omega}_e(\beta)}{\hat{\omega}_i}, \tag{20}$$

r_i being related to the electrical frequency ω_e and $\bar{r}_i$ its modified version due to the detuning brought by the nonsmooth term. One arrives at the following system:

$$\ddot{\tilde{q}}_i + 2\xi_i\dot{\tilde{q}}_i + \tilde{q}_i + \bar{k}_i\bar{r}_i\tilde{Q} = f_i\cos\tilde{\Omega}\tilde{t}, \tag{21a}$$

$$\ddot{\tilde{Q}} + 2\bar{\xi}_e\bar{r}_i\dot{\tilde{Q}} + \bar{r}_i^2\tilde{Q} + \bar{k}_i\bar{r}_i\tilde{q}_i = 0, \tag{21b}$$

where the derivatives are with respect to the dimensionless time τ. $\bar{k}_i$ is the modified dimensionless electromechanical modal coupling factor due to the presence of the nonsmooth term defined as:

$$\bar{k}_i(\beta) = k_i\sqrt{\phi_1(\beta)}. \tag{22}$$

Note that $\bar{k}_i$ depends on β, as suggested by the expression of ϕ_p in Eq. (17). More importantly, $\bar{k}_i$ is *smaller than the unmodified coupling factor* k_i since $\phi_1 < 1$ for for any nonzero value of β, as illustrated in Fig. 7. The physical meaning of this observation is that the nonsmooth term leads to a distribution of the energy to different harmonics, contrary to the linear case, where all the energy is transferred to the fundamental harmonic. Thus, a reduction of energy in the H1 harmonic is observed and quantified by the gain ϕ_1.

The FRFs of Eqs. (18a,b) reads:

$$H_q(\Omega) = \frac{\mathring{q}}{F} = \frac{1}{m_i}\frac{\bar{\omega}_e^2 - \Omega^2 + 2j\bar{\xi}_e\bar{\omega}_e\Omega}{D(\Omega)}, \quad H_Q(\Omega) = \frac{\mathring{Q}}{F} = \frac{-\bar{\omega}_e^2\phi_1\theta_i}{m_i}\frac{1}{D(\Omega)}, \tag{23}$$

with $D(\Omega) = (\hat{\omega}_i^2 - \Omega^2 + 2j\xi_i\hat{\omega}_i\Omega)(\bar{\omega}_e^2 - \Omega^2 + 2j\bar{\xi}_e\bar{\omega}_e\Omega) - \bar{k}_i^2\bar{\omega}_e^2\hat{\omega}_i^2$ and where $\mathring{q}$ and $\mathring{Q}$ are the Fourier transform of $q(t)$ and $Q(t)$, respectively.

3.1.2 Optimal tuning

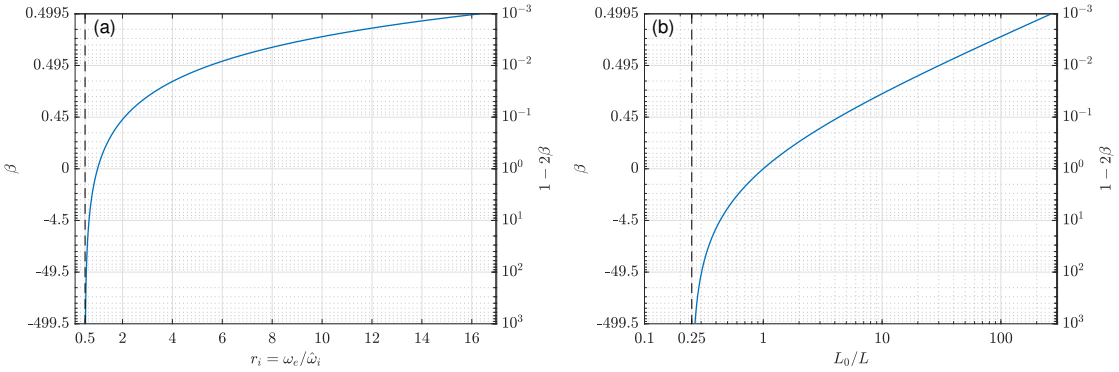

Fig. 8: Optimal value β^{op} of β to tune the RL-shunt as a function of (a) $r_i = \omega_e/\hat{\omega}_i$ and (b) as a function of the reduction ratio of the shunt inductance with respect to its optimal value for a linear RL-shunt L_0/L.

To obtain the optimal response of our modified RL-shunt, we follow the same optimization procedure as the one used for classical RL-shunts [2], as recalled in Appendix A. Comparing Eqs. (21) and (A.1), one observes that $(\bar{\omega}_e, \bar{k}_i, \bar{\xi}_e)$ replace (ω_e, k_i, ξ_e). Considering first the frequency tuning, the optimal value for the modified electrical frequency, denoted by $\bar{\omega}_e^{\text{op}}$, should satisfy:

$$\bar{\omega}_e^{\text{op}} = \hat{\omega}_i \quad \Rightarrow \quad \bar{r}_i^{\text{op}} = 1. \tag{24}$$

Then, by substituting $\bar{\omega}_e$ from Eq. (11) in Eqs. (24), one arrives to the following optimal value of β, denoted by β^{op}, as a function of the unmodified electrical tuning ratio $r_i = \omega_e/\hat{\omega}_i$:

$$\eta^{\text{op}} = \frac{\bar{\omega}_e^{\text{op}}}{\omega_e} = \frac{\hat{\omega}_i}{\omega_e} = \frac{1}{r_i} \quad \Rightarrow \quad \beta^{\text{op}} = \frac{1}{2}\left[1 - \frac{1}{(2r_i - 1)^2}\right]. \tag{25}$$

Notice that (see Fig. 2(b)):

$$r_i \in [1, +\infty] \quad \Leftrightarrow \quad \eta \in [0, 1] \quad \Leftrightarrow \quad \beta \in [0, 0.5], \tag{26a}$$
$$r_i \in [0.5, 1] \quad \Leftrightarrow \quad \eta \in [1, 2] \quad \Leftrightarrow \quad \beta \in [-\infty, 0], \tag{26b}$$

such that r_i is necessary larger than 0.5.

The above equations show that the nonsmooth component brings a new degree of freedom in the tuning of the resonant shunt. In practice, one can adjust the value of the nonlinear gain such that $\beta = \beta^{\text{op}}$ (Eq. (25)), bringing the modified electrical frequency close to the mechanical one, such that $\bar{\omega}_e = \hat{\omega}_i$ ($\bar{r}_i = 1$). In practice, a standard RL-shunt is tuned using the value L of the inductance, such that the electrical frequency is equal to the open-circuit mechanical one: $\omega_e = 1/\sqrt{LC_{\text{p}i}} = \hat{\omega}_i$. Here, adjusting the value of β is an additional degree of freedom to tune the RL-shunt. The range of tuning can be such that $\omega_e > \hat{\omega}_i$ ($r_i > 1$): in this case $\beta^{\text{op}} > 0$; on the contrary, one can have $\hat{\omega}_i/2 < \omega_e < \hat{\omega}_i$, leading to $\beta^{\text{op}} < 0$. This is illustrated in Fig. 8(a), which shows the evolution of β^{op} as a function of r_i.

This new degree of freedom can be used in practice to finely adjust the tuning of an RL-shunt that has a nonoptimal value of the inductance L. It can also be used intentionally in the case of a low-frequency mechanical mode that would require a high value of L, often difficult to achieve in practice.

In this case, one chooses a smaller L than the optimal one and corrects the tuning by adjusting β. To clarify the reduction in L, we compare it with the required inductance for the optimal condition of the linear RL-shunt (see Appendix A), denoted by L_0. Considering that $\omega_e = 1/\sqrt{LC_{\mathrm{pi}}}$, one has:

$$\frac{L}{L_0} = \left(\frac{\bar{\omega}_e}{\omega_e}\right)^2 = \frac{1}{r_i^2} \quad \Rightarrow \quad L = \frac{L_0}{r_i^2}. \tag{27}$$

Thus, the inductance can be reduced by a factor of r_i^2 compared to that of the linear RL-shunt. This quadratic law can be very advantageous in practice: for instance, a value of $r_i = 10$ leads to a reduction in the inductance of a factor $L_0/L = 100$. This is illustrated in Fig. 8(b), which shows β^{op} as a function of L_0/L.

In addition to the frequency tuning, the electrical damping must also be tuned. The optimal value of the electrical damping ratio ξ_e and thus of the resistor R are obtained by:

$$\bar{\xi}_e^{\mathrm{op}} = \frac{\sqrt{6}\bar{k}_i}{4} \quad \Rightarrow \quad \xi_e^{\mathrm{op}} = \eta^{\mathrm{op}}\bar{\xi}_e^{\mathrm{op}} = \frac{\sqrt{6}}{4r_i}\bar{k}_i = \frac{\sqrt{6}}{4r_i}k_i\sqrt{\phi_1^{\mathrm{op}}} \quad \Rightarrow \quad R^{\mathrm{op}} = \frac{\sqrt{6}}{2C_{\mathrm{pi}}r_i^2\hat{\omega}_i}k_i\sqrt{\phi_1^{\mathrm{op}}}, \tag{28}$$

where $\phi_1^{op} = \phi_1(\beta = \beta^{\mathrm{op}})$ as defined by Eq. (17). Contrary to the linear RL-shunt, the optimal damping ratio ξ_e^{op} do not depend only on the coupling factor k_i, but also on the linear tuning $r_i = \omega_e/\hat{\omega}_i$ of the shunt, since ϕ_1^{op} depends on r_i through β^{op} (Eq. (25)):

$$\phi_1^{\mathrm{op}} = \sum_{m=0}^{4} a_m \left[2\log_{10}(2r_i - 1)\right]^m, \tag{29}$$

where a_m are defined in Table 1 for the first harmonic and for $\beta > 0$ ($r_i > 1$). For $\beta < 0$ ($0.5 < r_i < 1$), one must change the sign of a_m for m even, as explained in section 2.2.3.

3.1.3 Performance

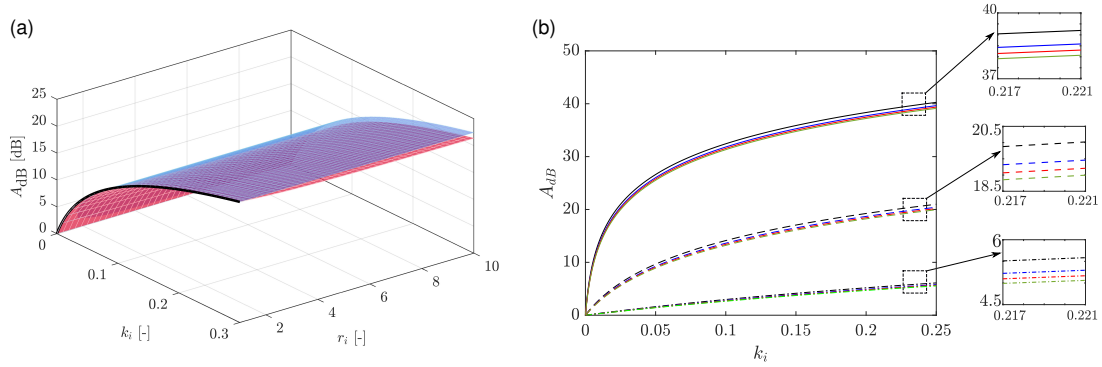

Fig. 9: Optimal attenuation A_{dB} as a function of r_i and k_i. (a) 3D plot for a linear RL-shunt (blue surface, $\beta = 0$) and for the 1:1 tuning case with the nonsmooth component (red surface), for $\xi_i = 0.01$. The black line denotes the intersection between the two surfaces at $r_i = 1$; (b) A_{dB} as function of k_i for $\xi_i = 0.001$ (solid lines), $\xi_i = 0.01$ (dashed lines), and $\xi_i = 0.1$ (dashed-dotted lines) and for each value of ξ_i, for three different values of r_i: $r_i = 10$ (in green), $r_i = 5$ (in red), $r_i = 2$ (in blue), and $r_i = 1$ (in black). The case for $r_i = 1$ denotes also the linear resonant shunt since $\beta = 0$.

The optimal attenuation $A_{\rm dB}$ of the nonlinear RL-shunt, in dB scale, can be obtained using the procedure of Appendix A by replacing k_i by its modified value $\bar{k}_i$. It reads:

$$A_{\rm dB} = 20\log_{10}\frac{H_q|_{\bar{k}_i=0}(\tilde{\Omega}=1)}{H_q|_{\bar{\xi}_e=\bar{\xi}_e^{\rm op}\bar{r}_i=1}(\tilde{\Omega}=1)} = 20\log_{10}\left(1+\frac{\bar{k}_i}{\xi_i\sqrt{6}}\right) = 20\log_{10}\left(1+\frac{k_i\sqrt{\phi_1^{\rm op}}}{\xi_i\sqrt{6}}\right). \quad (30)$$

By substituting Eq. (29) in Eq. (30), we can conclude that in contrary to the linear resonant shunt case where only k_i and ξ_i are involved, the optimal attenuation depends also on the ratio r_i (and thus on the inductance). In addition, one can expect a reduction of $A_{\rm dB}$ as β increases due to the reduction of k_i by a factor of $\sqrt{\phi_1}$.

The dependence of $A_{\rm dB}$ on (k_i, ξ_i, r_i) is examined in Fig. 9. Classically, one observe that $A_{\rm dB}$ increases as a function of the coupling factor k_i and when the mechanical damping ratio ξ_i is decreased, in the same way than for a linear RL-shunt (see Fig. 24 in Appendix A and [2]). On the contrary, the effect of the nonsmooth term on $A_{\rm dB}$ appears through its dependence on the tuning ratio r_i through $\phi_1^{\rm op} = \phi_1(\beta^{\rm op})$. Fig. 9 clearly show that this dependence on r_i is very weak since $A_{\rm dB}$ is only slightly reduced with respect to the linear RL-shunt (with $\beta = 0 \Leftrightarrow r_i = 1$). This is an excellent result since the huge benefit of being able to decrease a lot the inductance L ($r_i = 10 \Leftrightarrow L = L_0/100$) is not counterbalanced by a significant decrease of the performance, of the order of 1 dB.

3.1.4 Numerical validation

In this section, we numerically validate the frequency response and the optimal parameters of our modified RL-shunt by considering the first twisting mode of the hydrofoil structure that will be tested experimentally in section 4 (see Fig. 17). The modal parameters corresponding to this mode are gathered in Table. 3. The numerical results are obtained by solving Eq. (7a,b) with MANLAB, considering 40 harmonics in the simulations. Then, the frequency responses of the first harmonic amplitude of the displacement $u_{\rm H1}$, the charge $Q_{\rm H1}$, and the PE voltage $V_{\rm H1}$ are obtained. Note that in what follows, the modal parameters correspond to this particular mode, and thus *the subscript i associated with the modal parameters notations is omitted in the remaining of this section*. Note also that the modal parameters are gathered in Table. 3 follow the normalization of the mode shape such that $\psi = 1$ at the point of the structure where the displacement is studied and thus according to Eq. (1), we have $u(t) = q(t)$.

As a first step, we choose the inductance L such that $\omega_e = 2\hat{\omega}$ (*i.e.* $r = 2$ and $L = 0.737$ H), meaning that the linear RL-shunt is overtuned by a factor 2. We correct this overtuning by adjusting the other parameters at their optimal value: $\beta = \beta^{\rm op} = 0.444$ (Eq. (25)) and $\xi_e = \xi_e^{\rm op}$ (Eq. (28)). The first harmonics of $u(t)$ and $Q(t)$ in the periodic steady state are shown in Figs. 10(a,b) as a function of the driving frequency Ω, for three values of the forcing F. Then, in Figs. 10(c,d), the same curves are plotted normalized by the forcing level F and superimposed to the FRFs $H_q(\Omega)$ and $H_Q(\Omega)$ (Eqs. (23)) of the linear equivalent system (18a,b). One observes a perfect match, proving first that the linearity of the response with respect to the excitation level is perfect, as well as the agreement between the full nonlinear system (7a,b) and its linear approximation (18a,b).

Fig. 11 is analogous to Fig. 10(c,d) and shows how the frequency responses are changed when the parameters β and ξ_e are changed around their optimal values $\beta^{\rm op}$ and $\xi_e^{\rm op}$. Note that we chose to plot $V_{\rm H1}$ instead of $Q_{\rm H1}$ since obtaining the order of magnitudes of the voltage will be useful for the practical realization of the shunt circuit. Those plots are similar to the response of a linear RL-shunt when ω_e and ξ_e are varied around their optimal value, showing again the equivalence of our modified RL-shunt to a classical linear RL-shunt.

To validate numerically the dependence of the optimal attenuation on the frequency ratio r and, thus the inductance, as suggested in Figs. 9(a,b), Fig. 12(a) shows the numerical frequency response of $u_{\rm H1}$ normalized with respect to the forcing level for different values of r in which the optimal

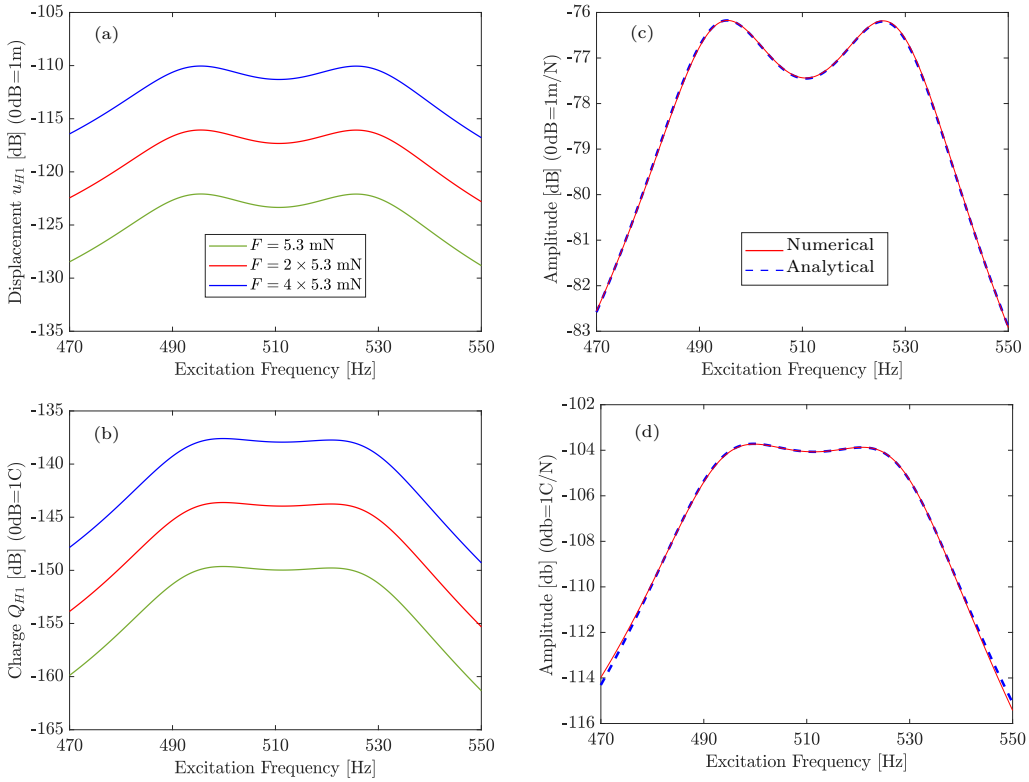

Fig. 10: (a,b): Numerical frequency response of the first harmonics u_{H1} and Q_{H1} of $u(t)$ and $Q(t)$ for increasing excitation levels; (c,d) superposition of analytical ($H_q(\Omega)$ and $H_Q(\Omega)$ from (23a,b) in dashed blue line) and numerical (u_{H1}/F and Q_{H1}/F in solid red line) frequency responses normalized with respect to the forcing. In the plots, optimal values are used such that $\beta = \beta^{\mathrm{op}} = 0.444$ $R = R^{\mathrm{op}} = 237.58\Omega$, estimated from Eq. (25) and Eq. (28), respectively. The modal parameters used are the ones gathered in Table. 3 and $L = 0.737\mathrm{H} \Leftrightarrow r = \omega_e/\hat{\omega} = 2$.

conditions are always satisfied (i.e., for each value of r we set $R = R^{\mathrm{op}}$, $\beta = \beta^{\mathrm{op}} \Rightarrow \bar{\omega}_e = \hat{\omega}$). Similar to Fig. 11, we consider the first twisting mode of the hydrofoil structure shown in Fig. 17. The results validate that tuning r to higher values, and thus lower inductance, reduces the optimal attenuation with respect to that of the RL-shunt while preserving the response shape. In addition, Fig. 12(b) shows the optimal attenuation A_{dB} as function of r for the RL-shunt with $\beta = 0$ (Eq. (A.4)) and for the shunt with the nonsmooth term Eq. (30). Compatible with the results in Figs. 9(a,b), the results clearly show that for higher values of r (lower values of inductance), the optimal attenuation is slightly decreased, compared to the linear RL-shunt, by $\simeq$ 1dB for a reduction of the inductance by a factor of 100 for $r = 10$, compatible with results in Figs. 9(a,b). One can note that the attenuation predicted in Eq. (30) is numerically validated by a comparison with that obtained numerically, where an excellent fitting is obtained for different values of r. Note that the numerical attenuation, shown in circle markers in Fig. (12b), is directly deduced from Fig. 12(a) by the amplitude difference in dB scale between the open circuit frequency and the optimal response at $\Omega = \bar{\omega}_e$.

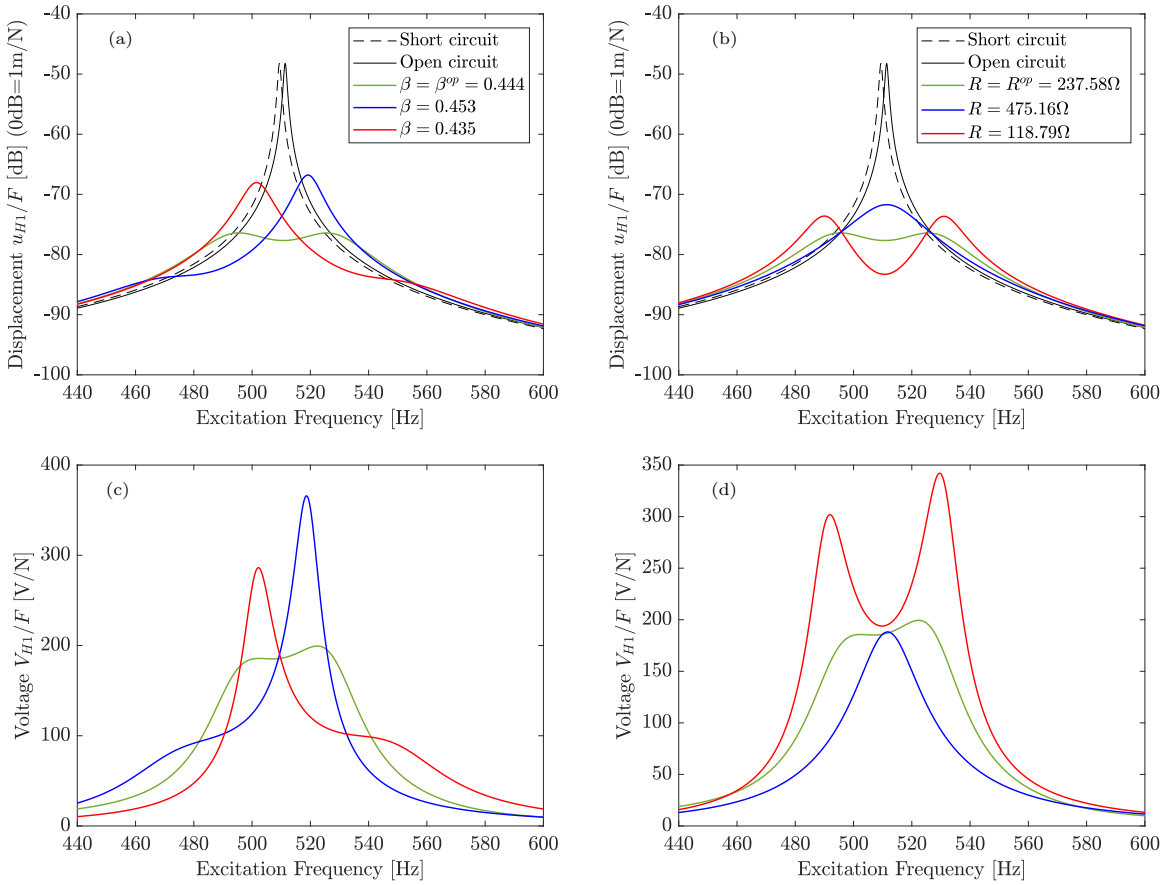

Fig. 11: Numerical frequency response of the first harmonics of u_{H1} (a,b) and V_{H1} (c,d) of $u(t)$ and $V(t)$, both normalized by the excitation level F. The response is shown for different values of β with $R = R^{\mathrm{op}} = 237.58\Omega$ (a,c) and different values of R with $\beta = \beta^{\mathrm{op}} = 0.444$ (b,d). The modal parameters used are the ones gathered in Table. 3 and $L = 0.737\mathrm{H} \Leftrightarrow r = \omega_e/\hat{\omega} = 2$.

3.2 One-to-two tuning of the nonlinear shunt ($\bar{\omega}_e = 1/2\hat{\omega}$)

In this section, we examine another possible tuning denoted by two-to-one (2:1) tuning such that $\bar{\omega}_e = \hat{\omega}_i/2$. Due to the nonlinearities generated by the nonsmooth term, this tuning is expected to activate a nonlinear modal coupling through a 2:1 internal resonance. As discussed in [19, 20], if quadratic nonlinear terms are present in $V_{\mathrm{nl}}(t)$, the 2:1 internal resonance leads to create an antiresonance at which the amplitude of the host structure becomes independent of the forcing level, a so-called saturation phenomenon. In this section, we investigate the behavior of our system (which includes a nonsmooth nonlinearity and not a quadratic one) in the same internal resonance condition.

3.2.1 Validation of the occurrence of the 2:1 internal resonance

To validate the energy transfer through the 2:1 internal resonance, we focus on the first harmonic response of the displacement amplitude u_{H1} and the first subharmonic response of the charge $Q_{\mathrm{H1/2}}$. We consider them dominant in the Fourier series like in a classical 2:1 internal resonance energy

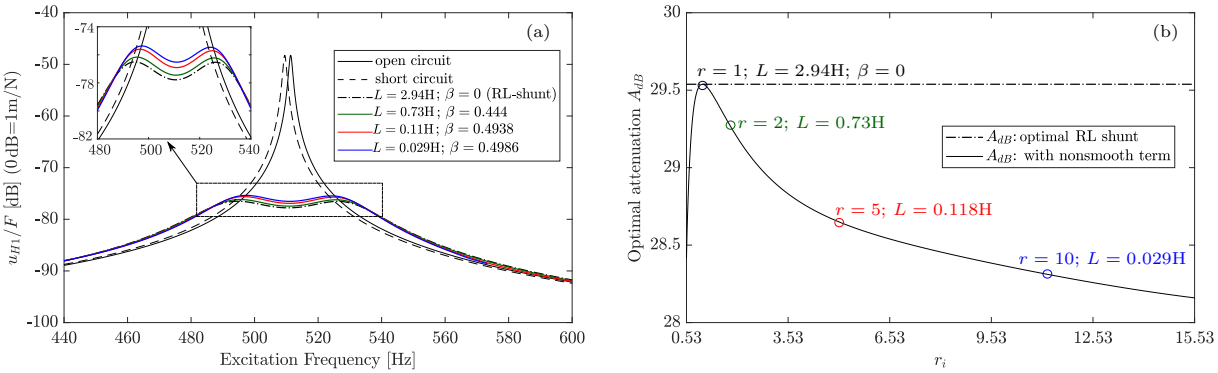

Fig. 12: (a) Numerical frequency response of the first harmonic u_{H1} of the displacement $u(t)$, normalized with respect to the forcing level F, for different values of the ratio r and by satisfying the optimal conditions in Eq. (25) and Eq. (28). (b) Optimal attenuation for the case of RL-shunt (Eq. (A.4)) and the case with the nonsmooth component with one to one tuning (Eq. (30)). The circle markers are the attenuation obtained numerical frequency responses for each value of r. The modal parameters used are the ones gathered in Table. (3).

transfer (see [19]) and we express $u(t)$ and $Q(t)$ as:

$$u(t) = u_{\mathrm{H1}} \cos\left(\Omega t - \gamma_2\right) + \mathrm{oh}, \tag{31a}$$

$$Q(t) = Q_{\mathrm{H1/2}} \cos\left(\frac{\Omega}{2} t - \frac{\gamma_1 + \gamma_2}{2}\right) + \mathrm{oh}, \tag{31b}$$

where "oh" denotes other harmonics, including the contribution of the H0 and H2 harmonics due to the presence of the nonsmooth term. γ_2 is the phase angle of the first harmonic of the displacement with respect to the forcing, and γ_1 can be considered as the relative phase angle between the two oscillators, which is proved to be locked at $3\pi/2$ at the antiresonance frequency in the case of 2:1 internal resonance [19].

Similar to the 1:1 tuning case in section 3.1, the electrical frequency is tuned according to the nonsmooth gain β with no condition on the inductance value. Thus, the 2:1 tuning condition requires tuning β as:

$$\bar{\omega}_e = \frac{1}{2}\hat{\omega} \quad \Rightarrow \quad \beta = \frac{1}{2}\left[1 - \left(\frac{1}{4r_i - 1}\right)^2\right] \tag{32}$$

To test the ability of activating the 2:1 internal resonance, we solve numerically the system (2a,b) by setting β according to Eq. (32) with an arbitrary low electrical damping ratio and using the modal parameters in Table. 3. In addition, the inductance $L = 2.948$ H is chosen to have $r = \omega_e/\hat{\omega} = 1$. The results are shown in Fig. 13, which clearly shows that a nonlinear energy transfer occurs from the first harmonics H1 of $u(t)$ to the subharmonic H1/2 of $Q(t)$. This energy transfer occurs after pitchfork bifurcation "PF" (or period-doubling bifurcation), in a frequency band centered around the mechanical resonance, at $\Omega \simeq \hat{\omega}_i$.

However, contrary to a classical 2:1 internal resonance produced by quadratic nonlinear terms (as in [19]), the topology of the coupled response curve is completely different and *does not show any saturation phenomenon.* They appear with a shape very close to the response of a linear RL-shunt. This suggests to consider the second harmonic of $Q(t)$ (which is H1 here) as *an equivalent linear oscillator that can be optimized as a classical RL-shunt to mitigate the resonance of the i-th mode of the host structure.* Following this idea, as seen in Fig. 13(a), the tuning of β according to Eq. (32)

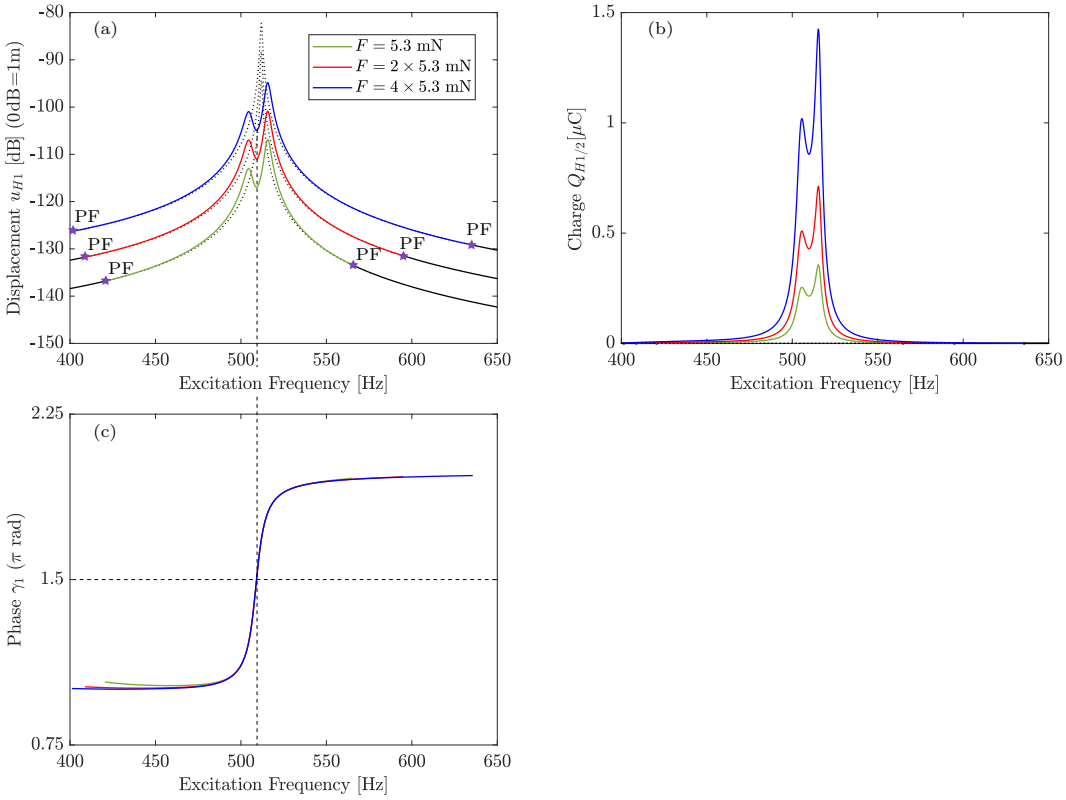

Fig. 13: (a) and (b) show respectively the numerical frequency response of u_{H1} and $Q_{\mathrm{H1/2}}$ for increasing excitation levels. (c) shows the relative phase γ_1 between the two oscillators. The linear response is plotted in black. The stable and unstable responses are depicted in solid and dotted lines, respectively. The purple star denotes the pitchfork bifurcation (PF). The numerical values used are $\beta = 0.444$, $R = 36\Omega$, $L = 2.948$H. The modal parameters used are the ones gathered in Table. 3.

and the chosen ξ_e do not lead to an optimal response, that would be characterized by a symmetric shape and minimal peaks, as observed in Fig. 11 for the 1:1 tuning case. Thus, an optimization study is necessary to obtain the optimal values of β and ξ_e to achieve an optimal attenuation similar to that of a linear RL-shunt.

Another important feature concerns the relative phase γ_1 that locks at $3\pi/2$ at the antiresonance frequency, independent from the excitation level. This feature was proved analytically and numerically in [19] with the addition of quadratic nonlinearities in the shunt circuit. As seen in Fig 13c, the same phase lockage is equally preserved, which can be exploited for tuning the system in practical implementation, similar to the experimental study in [20].

3.2.2 Optimization study

Similar to the case with 1:1 tuning, the optimization is established through the nonsmooth gain β to tune the electrical resonance frequency and the electrical damping ratio ξ_e (thus the resistance R), to obtain a mechanical frequency response as low and flat as possible. Two points are considered for this optimization: (i) we are looking for an optimal value of β that symmetrizes the frequency response,

as for a classical RL-shunt; (ii) the coupled response is obtained through a 2:1 internal resonance, as observed in the previous section.

As shown in [19], the symmetric response with a 2:1 internal resonance requires a ratio between the electrical frequency $\bar{\omega}_e$ and the mechanical one $\hat{\omega}_i$ to be slightly higher than half (i.e., contrary to the tuning in (Eq. (32)). The exact value of this ratio, denoted by r_i^*, can be estimated by setting $\omega_2 = 2\omega_1$ where ω_2 and ω_1 are the natural frequencies in the electro-mechanical basis (see Appendix C and [19]). The obtained r_i^* depends only on the piezoelectric coupling factor k_i as follows:

$$r_i^* = \sqrt{\frac{1}{8}\left(17 - 25k_i^2 - 5\sqrt{25k_i^4 - 34k_i^2 + 9}\right)}. \tag{33}$$

Given the value of r_i^*, the optimal value of β is then estimated as:

$$\bar{\omega}_e^{\mathrm{op}} = r_i^*\hat{\omega}_i \quad \Rightarrow \quad \eta^{op} = \frac{r_i^*}{r_i} \quad \Rightarrow \quad \beta^{\mathrm{op}} = \frac{1}{2}\left[1 - \left(\frac{r_i^*}{2r_i - r_i^*}\right)^2\right] \tag{34}$$

Since it is the second harmonics of the charge $Q(t)$ that is coupled to the primary (mechanical) oscillator, we consider for the optimization its equivalent linear oscillator, as defined by Eq. (14) in section 2.2.3 with $p = 2$. Thus, the key point is to modify the piezoelectric coupling through the gain ϕ_2. Following the same reasoning as in section 3.1.1, the modified PE coupling factor for the two-to-one tuning case can be expressed as:

$$\bar{k_i}^* = k_i\sqrt{\phi_2(\beta)}. \tag{35}$$

We then express the optimal value of ξ_e (and the resistance R) as follows:

$$\bar{\xi}_e^{\mathrm{op}} = \frac{\sqrt{6}}{4}\bar{k}_i^*, \quad \Rightarrow \quad \xi_e^{\mathrm{op}} = \frac{\sqrt{6}r_i^*\bar{k}_i^*}{4r_i} = \frac{\sqrt{6}r_i^*k_i\sqrt{\phi_2^{\mathrm{op}}}}{4r_i} \quad \Rightarrow \quad R^{\mathrm{op}} = \frac{\sqrt{6}r_i^*}{2C_{\mathrm{p}_i}r_i^2\hat{\omega}_i}k_i\sqrt{\phi_2^{\mathrm{op}}}, \tag{36}$$

where $\phi_2^{op} = \phi_2(\beta = \beta^{\mathrm{op}})$ to satisfy the optimal conditions. Considering Eq. (17) and (34), on has:

$$\phi_2^{\mathrm{op}} = \sum_{m=0}^{6} a_m\left[2\log_{10}\left(\frac{2r_i - r_i^*}{r_i^*}\right)\right]^m, \tag{37}$$

where a_m are defined in Table 1 for the second harmonic. The optimal attenuation can then be expressed as:

$$A_{\mathrm{dB}} = 20\log_{10}\left(1 + \frac{\bar{k_i}^*}{\xi_i\sqrt{6}}\right) = 20\log_{10}\left(1 + \frac{k_i\sqrt{\phi_2^{\mathrm{op}}}}{\xi_i\sqrt{6}}\right). \tag{38}$$

Similar to 1:1 tuning case, the optimal attenuation depends explicitly on r_i (thus the inductance) but with a reduction of the piezoelectric coupling factor by $\sqrt{\phi_2}$. Thus, a further reduction of the attenuation compared to that of the linear resonant shunt is expected since ϕ_2 admits an order of magnitude lower than that of ϕ_1, as suggested in Fig. 7. This is further illustrated in Fig. 14 by comparing A_{dB} of the 2:1 tuning case and that of a linear RL-shunt.

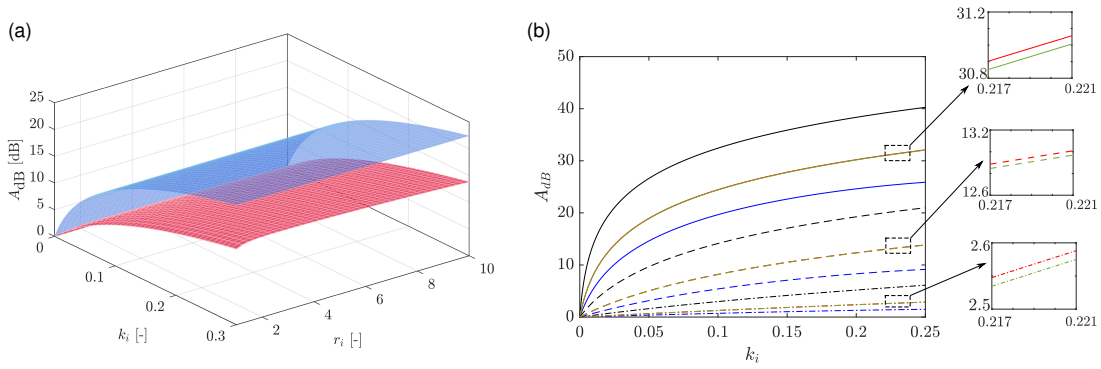

Fig. 14: Optimal attenuation A_{dB} as a function of r_i and k_i. (a) 3D plot for a linear RL-shunt (blue surface, $\beta = 0$) and for the 2:1 tuning case with the nonsmooth component (red surface), for $\xi_i = 0.01$; (b) A_{dB} as function of k_i for $\xi_i = 0.001$ (solid lines), $\xi_i = 0.01$ (dashed lines), and $\xi_i = 0.1$ (dashed-dotted lines) and for each value of ξ_i, for three different values of r_i: $r_i = 10$ (in green), $r_i = 5$ (in red), $r_i = 2$ (in blue), and $r_i = 1$ (in black). The case for $r_i = 1$ denotes also the linear resonant shunt since $\beta = 0$.

3.2.3 Numerical validation

In order to validate the results suggested from the optimal analysis, we solve numerically the system (7a,b) to obtain the frequency responses of u_{H1} and $V_{\mathrm{H1}/2}$ for different values of β and R (thus ξ_e) including the optimal conditions in Eq. (34) and Eq. (36), respectively. This is shown in Fig. 15 in which we choose the inductance such that $r = 1 \Leftrightarrow L = 2.948$ H.

Similar to the plots in section 3.1.4, we consider the first twisting mode of the foil shown in Fig. 17. The results clearly suggest that setting R and β according to the obtained optimal conditions enables the recovery of the symmetric behavior and the minimization of the peaks near the resonance frequency. It is worth mentioning that the response is very sensitive to any small perturbation of the optimal value of β (observe the very close values of β used in Figs. 15(a,c)).

Regarding the optimal attenuation, one can realize that Eq. (38) shares similar behavior compared to that of the 1:1 tuning case in Eq. (30) in which the attenuation depends on the inductance. However, as observed in Fig. 7 and contrary to the behavior of ϕ_1, the value of ϕ_2 increases with β then tends to admit a constant value as β increases. This suggests that *decreasing the inductance and thus the optimal value of β leads to enhancing the optimal attenuation*, contrary to the one-to-one tuning case. To validate this result, we perform a similar analysis to that in section 3.1.4 (in Fig. 12) by studying the frequency response of u_{H1} at the optimal condition with different values of the inductance. The numerical results in Fig. 16(a) clearly validate the increase of the attenuation as the inductance decreases, which can also be seen in Fig. 16(b), where the optimal attenuation is plotted versus the inductance value. In addition, it is realized that the attenuation increases up to a certain level where it remains almost constant as the inductance decreases. This behavior is explained by the presence of ϕ_2 in the optimal attenuation expression, which admits the same trend versus β as shown in Fig. 7. Moreover, comparing the numerical attenuation obtained numerically and analytically shows an excellent fitting, validating the attenuation expression in Eq. (38). It is also worth mentioning that the attenuation in this tuning case is reduced compared to the optimized RL-shunt with a narrower bandwidth due to the substantial reduction of the coupling factor suggested in Eq. (35) since ϕ_2 admits a very low amplitude.

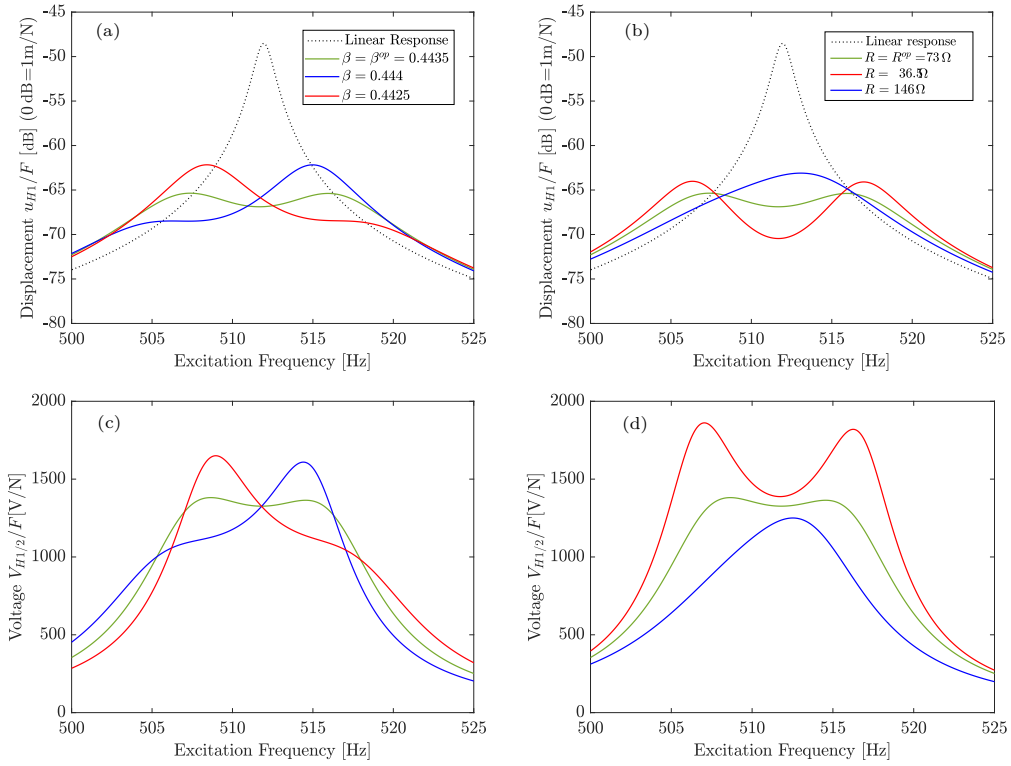

Fig. 15: Numerical frequency response of the first harmonic of the velocity u_{H1} (first row) and the PE voltage $V_{\mathrm{H1/2}}$ (second row), both normalized with respect to the excitation level. The response is shown for different values of β with $R = R^{\mathrm{op}} = 73\Omega$ (first column) and different values of R with $\beta = \beta^{\mathrm{op}} = 0.4435$ (second column). The inductance value used in the simulations is $L = 2.94\mathrm{H} \implies r = \omega_e/\hat{\omega} = 1$. The stable and unstable responses are depicted in solid and dotted lines, respectively. The displacement and voltage responses are plotted in dB and linear scales, respectively.

3.3 Summary

The introduced nonsmooth term enables tuning the electric resonance frequency of the shunt circuit while setting a low inductance in the circuit. In addition, it suggests a multi-harmonic response dominated by the zeroth, first, and second harmonics that appeared to be similar to that of a linear oscillator. In addition, strong nonlinearities appeared in the superharmonic response. A 1:1 and 2:1 tuning cases has been studied through the approximation of the main system (7a, b) to an approximated system in (18a,b) by modifying (and reducing) the piezoelectric coupling factor by $\sqrt{\phi_1}$ and $\sqrt{\phi_2}$ for the 1:1 and 2:1 tuning, respectively. In either case, closed-form expressions of the optimal values of β and R in addition to optimal attenuation are determined and gathered in Table. 2. Contrary to the linear resonant shunt, the frequency ratio r_i (thus the inductance) appears explicitly in the attenuation expression. The 1:1 tuning case shows an important feature in which one can reduce the required inductance by a factor of 100 for an attenuation reduction around 1dB compared to that of a linear resonant shunt. While for the 2:1 tuning case, a substantial reduction of the attenuation is observed but with an interesting feature in which the attenuation increases with the reduction of the inductance up to a certain level where it stays almost constant. The analytical results were then validated numerically by applying the absorber to attenuate the first twisting mode of a hydrofoil

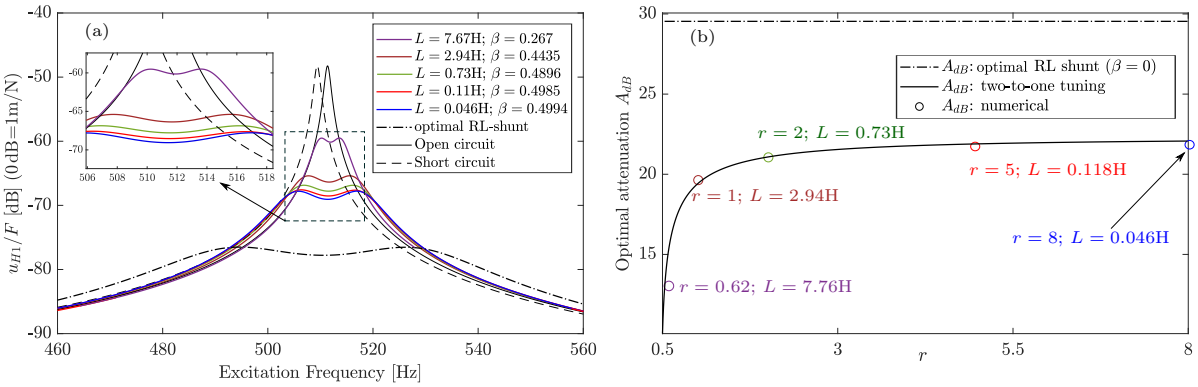

Fig. 16: (a) Frequency response of the first harmonic of the displacement, normalized with respect to the forcing level, for different values of the ratio r and by satisfying the optimal conditions in Eq. (34) and Eq. (36). (b) Optimal attenuation for the case of RL-shunt (Eq. (A.4)) and the case with the nonsmooth component with two to one tuning (Eq. (38)). The circle markers are the attenuation obtained numerical frequency responses for each value of r. The modal parameters used are the ones gathered in Table. (3).

structure. Considering also the first twisting mode of the hydrofoil, an experimental validation will be shown in the next section.

Table 2: Optimal parameters and optimal attenuation for the 1:1 and 2:1 tuning cases.

Case	Optimal β	Optimal R	Optimal attenuation [dB]
1:1 tuning	$\beta^{\text{op}} = \frac{1}{2}\left[1 - \left(\frac{1}{2r_i - 1}\right)^2\right]$	$R^{\text{op}} = \frac{\sqrt{6}}{2C_{\text{pi}} r_i^2 \hat{\omega}_i} k_i \sqrt{\phi_1^{\text{op}}}$	$A_{\text{dB}} = 20\log_{10}\left(1 + \frac{k_i}{\xi_i\sqrt{6}}\sqrt{\phi_1^{\text{op}}}\right)$
2:1 tuning	$\beta^{\text{op}} = \frac{1}{2}\left[1 - \left(\frac{r_i^*}{2r_i - r_i^*}\right)^2\right]$	$R^{\text{op}} = \frac{\sqrt{6} r_i^*}{2C_{\text{p}_i} r_i^2 \hat{\omega}_i} k_i \sqrt{\phi_2^{\text{op}}}$	$A_{\text{dB}} = 20\log_{10}\left(1 + \frac{k_i}{\xi_i\sqrt{6}}\sqrt{\phi_2^{\text{op}}}\right)$

4 Experimental Validation

4.1 Experimental setup

The experimental tests were conducted on a clamped-free foil structure fixed at its base in a vice, as shown in Fig. 17. This structure is similar to the one used in [22, 46]. Three PE patches are glued on cavities machined on the surfaces of the foil: on one face (denoted patches 1, 2), two P-876.A15 DuraAct polymer coated multi-layer piezoelectric patches are used for transduction with the first bending mode, whereas a macro-fiber composite M8557-F1 with 45° fiber orientation is used on the other face (denoted patch 3) for coupling with the first twisting mode. In all the tests of this article, only patch 3 is used since we focus on the first twisting mode. Consequently, patch 3 is connected

to the shunt circuit, and patch 1 and 2 are short-circuited. The three PE patches are from the PI Ceramic manufacturer.

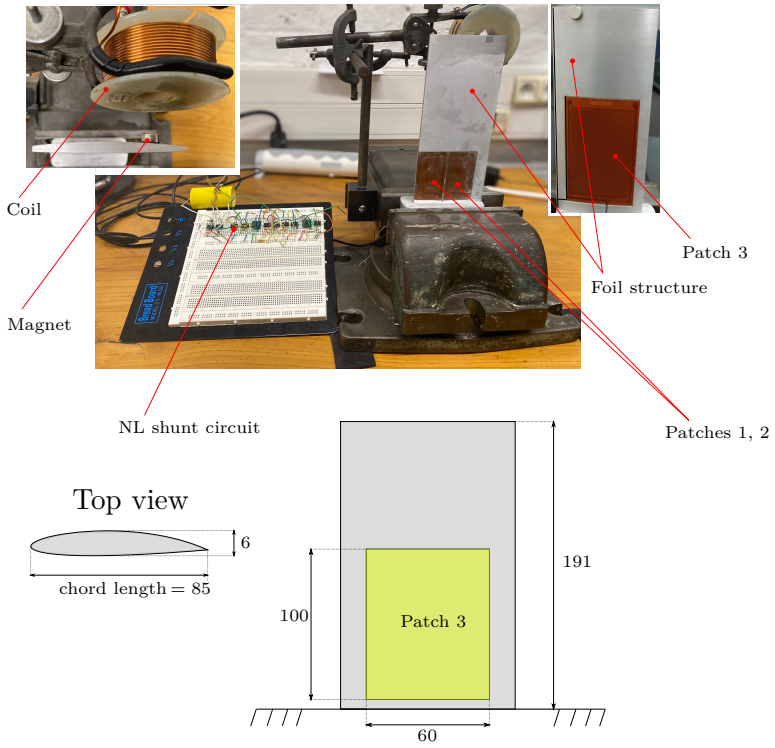

Fig. 17: Experimental Setup. Dimensions are in mm. The thickness of the PE patches is 1mm.

The mechanical excitation is realized by a coil interacting with a magnet fixed on the foil. The applied force is proportional to the current in the coil i.e $F(t) = \alpha I(t)$, where $\alpha = 0.6\ \mathrm{N\,A^{-1}}$ [20], with very low distortion [47]. A Brüel & Kjær 2719 power amplifier, connected to the coil, is used for all mechanical excitations. The foil vibrations are measured with a Polytec OFV-505 vibrometer, that provides the velocity of a point colocalized with the magnet location, close to the tip of the foil. Electrical measurements are performed using a PHILIPS PM 9355 precision current probe in the piezoelectric circuit to obtain the charge $Q(t)$ and a *Française d'Instrumentation* ST 500-5 differential voltage probe to measure the PE patch voltage $V(t)$.

To properly design the nonlinear shunt, we firstly performed an experimental modal analysis, equivalent to that in [20, 22], to obtain the modal characteristics of the first twisting mode of the foil, which are gathered in Table. 3. Note that since we tackle only the twisting mode, the subscript i will be omitted in what follows.

Table 3: Electro-mechanical modal parameters.

Parameter	$\breve{\omega}/(2\pi)$	$\hat{\omega}/(2\pi)$	ξ	m	C_p	θ	k	$\psi(\boldsymbol{x}_m)$
Value	509.4 Hz	511.36 Hz	0.0012	10.42 g	32.8 nF	5.2 mN/V	0.0875	1

Note that $\psi(\boldsymbol{x}_m) = 1$ means that the modal parameters are estimated by scaling the mode shape at the measurement point of the structure $\boldsymbol{x}_m$ to be unity, thus according to Eq. 1, $u(t) = q(t)$ (i.e., the same scaling of the mode shape considered in the previous section).

4.2 Nonsmooth shunt circuit

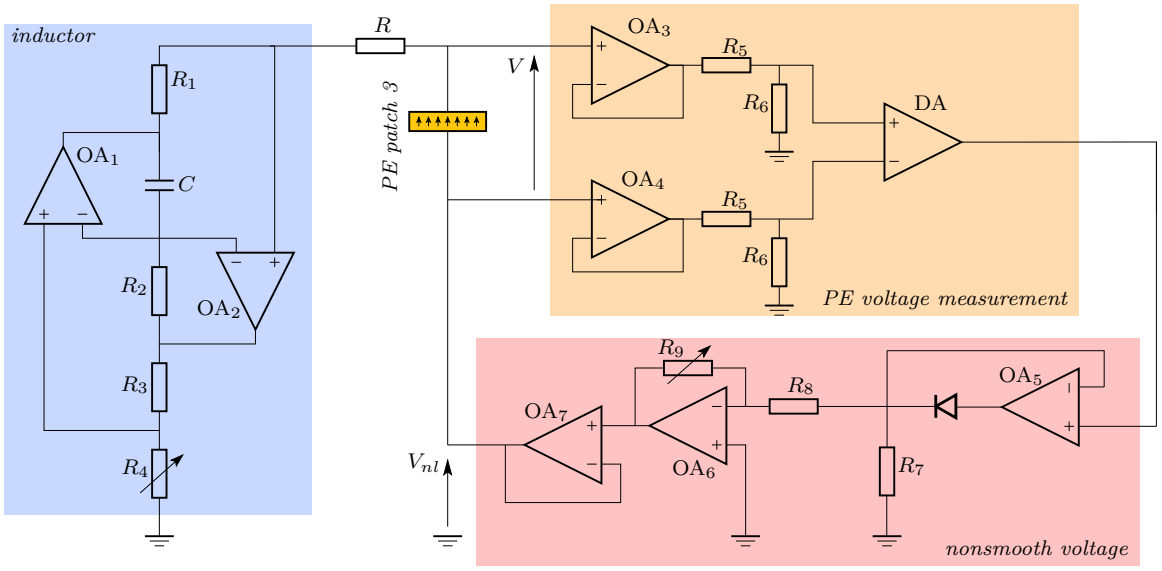

Fig. 18: Shunt circuit schematic.

Table 4: Component values in the nonlinear shunt circuit of Fig. 18

Component	R_1 [kΩ]	R_2 [kΩ]	R_3 [kΩ]	C [μF]	R_5 [kΩ]	R_6 [kΩ]	R_7 [kΩ]	R_8 [kΩ]
Value	2	1	1	10	82	22	10	10

The nonlinear shunt circuit used for the tests is shown in Fig. 18. It consists of three interconnected sub-circuits to realize (i) a tunable synthetic inductor (outlined in blue); (ii) a voltage measurement (outlined in orange), and (iii) a nonlinear voltage generator (outlined in light red). To handle the large voltage levels that can appear, especially during transients, the operational amplifiers OA_1 to OA_7 are OPA445 (Texas Instrument) which can operate up to ±40V and supply 15mA to drive the patches. The synthetic inductor is a so-called Antoniou circuit [48] to achieve the high inductance value needed to obtain an electrical resonance frequency close to half of the mechanical resonance frequency. The inductance value is given by

$$L = \frac{R_1 R_2 R_4 C}{R_3}, \tag{39}$$

where L is tuned using the variable resistance R_4.

As discussed in section 3, the *electric resonance frequency is controlled solely with the nonsmooth gain β according to a free choice of the inductance L*. In all the experimental tests in this study, and

for different tunings of the shunt circuit, the value of L is always chosen to be less than 3 H. For such values, the parasitic resistance generated by the Antoniou inductor, observed in [20], is to the order of 0.1Ω and will be neglected here. Thus, the resistor R in the shunt models corresponds to a physical resistance added to tune the electrical damping. Note that the parasitic resistance is estimated with a frequency-to-bandwidth ratio of the electrical resonance, close to $\Omega = \omega_e$, in linear operation, with $\beta = 0$.

The PE voltage measurement is established through two voltage dividers composed of R_5 and R_6 and two voltage followers OA_3 to OA_4 (OPA445, Texas Instrument) to ensure a large input impedance. The voltage dividers are used to attenuate the voltage to values compatible with the differential amplifier DA (INA826, Texas Instrument). Since the PE patch is not grounded, these voltages are first fed to the differential amplifier DA. The nonsmooth voltage with the absolute function, as in Eq. (6), is generated through a half-wave rectifier circuit composed of OA_5, a diode (1N4002), and a resistor R_7 connected to the ground. The output voltage of the half-wave rectifier circuit is fed to an inverting amplifier, realized with OA_6, to respect the assumed sign convention of the nonsmooth voltage in (2a,b) and to control the nonsmooth gain β. The follower OA_7 is used to minimize the output impedance while protecting the INA826 from excessive current. The nonsmooth gain β is controlled according to the variable resistor R_9 as:

$$\beta = \frac{1}{2}\left(\frac{R_6}{R_5 + R_6}\right)\frac{R_9}{R_8}. \tag{40}$$

Note that changing the sign of the nonsmooth voltage can be done by flipping the polarity of the diode without using the inverting amplifier. However, for such a case, the nonsmooth gain will be controlled either by a voltage divider composed of R_5 and R_6 or by adding a new voltage divider instead of the inverting amplifier. In the first case, and for certain values of β, one might risk achieving a voltage at the input of the DA higher than the operating levels. In the second case, a restriction on the value of β is presented. Thus, we prefer to use the inverting amplifier so that the sign convention is respected with easy controllability of the nonsmooth gain.

4.3 Measurement protocol

The experimental tests aim to verify the results suggested theoretically in section 3, and thus we consider the same tuning cases, namely, the 1:1 and 2:1 tuning. It is proved that the former case leads to a fully linear response near the resonance frequency while the latter activates the 2:1 internal resonance and thus leads to the response of the subharmonic of the charge. Since the mode shape is scaled to verify $\psi(\boldsymbol{x}_m) = 1$, we express the time signals of the displacement $u(t)$ and the charge $Q(t)$ for the 1:1 tuning as:

$$u(t) = u_{\mathrm{H1}}\cos(\Omega t - \delta_1) + \mathrm{oh}, \tag{41a}$$

$$Q(t) = Q_{\mathrm{H1}}\cos(\Omega t - \delta_2) + \mathrm{oh}, \tag{41b}$$

and for the 2:1 tuning case, we include the subharmonic response such that [19]:

$$u(t) = u_{\mathrm{H1}}\cos(\Omega t - \gamma_2) + u_{\mathrm{H1/2}}\cos\left(\frac{\Omega}{2}t - \frac{\gamma_1 + \gamma_2}{2}\right) + \mathrm{oh}, \tag{42a}$$

$$Q(t) = Q_{\mathrm{H1}}\cos(\Omega t - \gamma_2) + Q_{\mathrm{H1/2}}\cos\left(\frac{\Omega}{2}t - \frac{\gamma_1 + \gamma_2}{2}\right) + \mathrm{oh}, \tag{42b}$$

where u_{H1} and $u_{\mathrm{H1/2}}$ are respectively the amplitude of the first and subharmonic of the displacement and Q_{H1} and $Q_{\mathrm{H1/2}}$ are respectively the amplitude of the first and subharmonic of the charge. δ_1 and δ_2 are the phase angles of first harmonic of $u(t)$ and $Q(t)$ for 1:1 tuning case. γ_2 is the phase angle of

the first harmonic of $u(t)$ for the 2:1 tuning case. Note that δ_1, δ_2, and γ_2 are measured with respect to the forcing. γ_1 is the relative phase angle between the first and the subharmonic, which is estimated to be locked at $3\pi/2$ at the antiresonance frequency associated with the 2:1 internal resonance [19, 20]. "oh" denotes the other harmonics, in particular, the zeroth and the second harmonics, generated due to the nonsmooth component.

In practice, the amplitude and phase angles of the harmonics of $u(t)$ and $Q(t)$ can be obtained by measuring the foil tip velocity $v(t)$ with the laser vibrometer and the voltage across the PE patch terminals $V(t)$ using the differential voltage probe (see the procedure in [20]). In what follows, we chose to show the experimental frequency response of u_{H1}, instead of v_{H1}, in both tuning cases because it will be more convenient to validate the optimization results suggested theoretically (see Table. 2). In addition, we chose to show V_{H1} and $V_{\mathrm{H1/2}}$ in the 1:1 and 2:1 tuning cases, respectively, instead of Q_{H1} and $Q_{\mathrm{H1/2}}$, since it will be useful to obtain the voltage level to ensure that it does not exceed the operating limits of the operational and differential amplifiers in the shunt circuit (see Fig. 18). Indeed, the subharmonic response is measured for the 2:1 tuning case to validate the energy transfer and, thus, the activation of the 2:1 internal resonance.

Note that in either tuning case, the frequency responses will be shown normalized with respect to the forcing, following the results in section 3, which suggest that the response curves are linear with respect to the excitation. To estimate the forcing F in [N], the current I in the coil is measured using a PHILIPS PM 9355 precision current probe, then the relation $F = \alpha I$ is used.

To establish the amplitude and phase frequency responses, we consider two different procedures for the 1:1 and 2:1 tuning cases. In the former case, the frequency response is directly estimated by exciting the foil with a chirp signal of time-varied excitation frequency using the coil/magnet system. This method can be extended to realize the frequency response for the 1:1 tuning case since it is proved in section 3.1 that the response is fully linear near the resonance frequency (i.e., no bifurcations or change of stability). In addition, we consider the first harmonics to be dominant in comparison with the zeroth and second harmonics for the range of β used in this study. Thus, the multi-harmonic nature of the response at the steady state will not lead to a significant effect on the measured frequency response. In the 2:1 tuning case, the chirp signal method is not suitable due to the bifurcation and change of stability associated with the response. Thus the sine-stepped method is used instead, similar to that in [20]. Namely, a sine current with fixed intensity is fed to the coil/magnet device to generate a harmonic force $F = F_0 \cos \Omega t$. Then, the excitation frequency Ω is increased (or decreased) by steps, keeping the intensity fixed, sweeping a domain close to the resonance frequency of the first twisting mode of the foil. For each frequency, the harmonics amplitude and phases of the velocity (thus the displacement) and the PE voltage are extracted in the steady state using the demodulation technique explained in [20]. The input/output signals were synthesized/measured with National Instrument cards (NI-9234, NI-9263) driven by a Matlab program.

5 Experimental Results

5.1 Experimental validation of the theoretical results

In order to validate the numerical predictions in section 3 and, in particular, the estimated optimal parameters, a comparison between the numerical and experimental results is presented in Fig. 19 for the 1:1 and 2:1 tuning cases. In the former case, the frequency responses of u_{H1} and V_{H1} in addition to δ_1 are shown. In the latter case, u_{H1} and $V_{\mathrm{H1/2}}$ in addition to the phase γ_1 and γ_2 are presented. Moreover, in the 1:1 tuning case, the inductance $L = 0.73$H is chosen such that $r = \omega_e/\hat{\omega} = 2$ while for the 2:1 tuning case, $L = 2.94$H is chosen such that $r = \omega_e/\hat{\omega} = 1$. In either case, the values of β and R are set according to their optimal conditions gathered in Table 2.

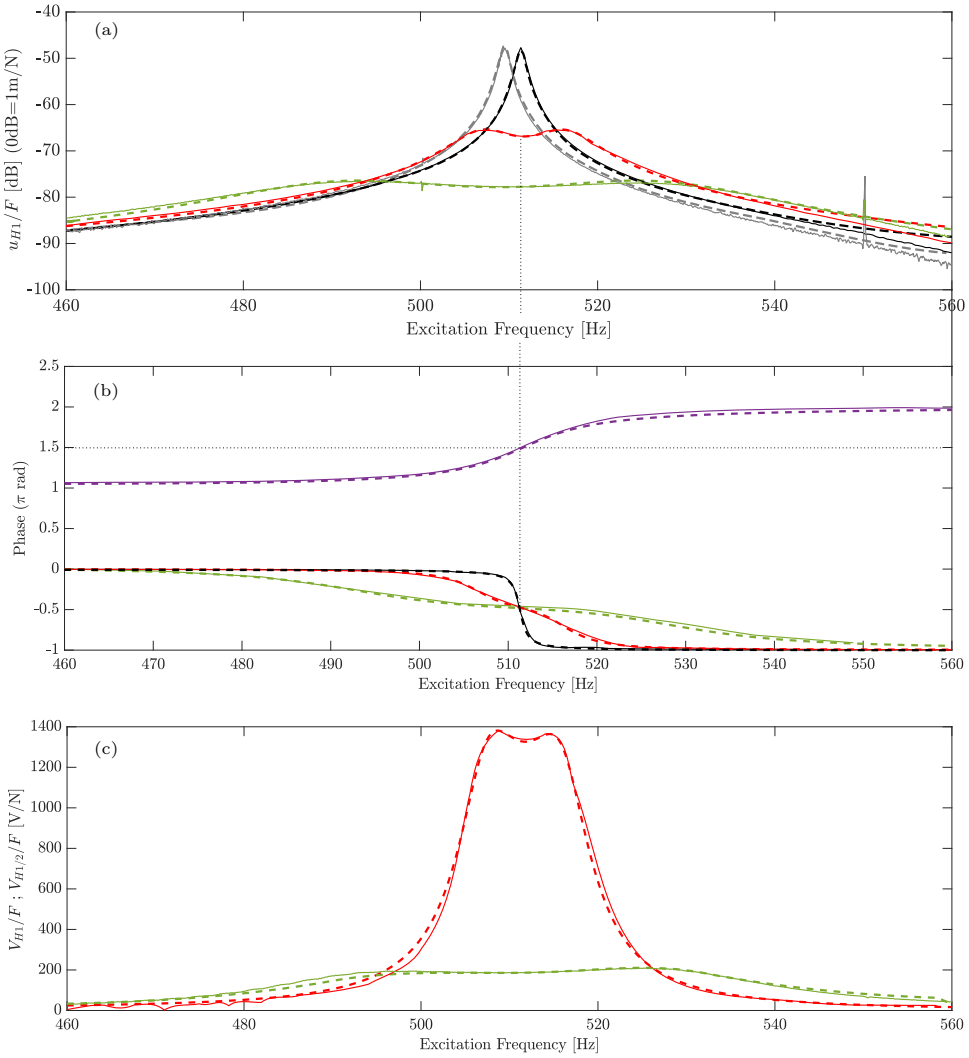

Fig. 19: Comparison between the numerical (dashed lines) and experimental (solid lines) frequency responses. In (a), the response of u_{H1} is shown for the 1:1 tuning (in green) and 2:1 tuning (in red), respectively. The short and open circuit responses are shown in gray and black lines, respectively. In (b), the phase δ_1 is shown for the linear case (in black) and for the 1:1 tuning (in green) in addition to γ_2 (in red) and γ_1 (in purple) for the 2:1 tuning. In (c), the responses of V_{H1} and $V_{\mathrm{H1/2}}$ are shown for the 1:1 tuning (in green) and 2:1 tuning (in red), respectively. For the 1:1 tuning case, we set $L = 0.73\mathrm{H}$,$\beta = \beta^{\mathrm{op}} = 0.444$, and $R = R^{\mathrm{op}} = 237.5\Omega$. For the 2:1 tuning case, we set $L = 2.94\mathrm{H}$,$\beta = \beta^{\mathrm{op}} = 0.4435$, and $R = R^{\mathrm{op}} = 73\Omega$. The modal parameters used in the numerical simulations are gathered in Table 3.

For completeness and comparison purposes, both the linear and the nonlinear frequency responses are depicted. The linear ones are estimated with the PE patch 3 in open and short circuit configurations. Comparing the numerical and the experimental results of the linear responses shows an excellent fitting validating the modal parameters estimated in Table 2 and the inductance tuning with the Antoniou inductor.

Regarding the nonlinear responses (i.e., with the nonsmooth component included in the shunt), the numerical and experimental frequency responses of the displacement, PE voltage, and phase angles suggest an excellent agreement for the 1:1 and 2:1 tuning cases. The following major points, suggested numerically in section 3, are validated: i) the response of u_{H1} for both tuning cases suggests a curve shape similar to that of the resonant shunt. ii) the estimated optimal parameters of β and R_e lead to the optimal response for both tuning cases since the response curves of u_{H1} show a symmetric behavior with respect to the resonance frequency with the amplitude of the two peaks around primary resonance is minimized. iii) Although an equivalent response shape compared to the RL-shunt is observed, the amplitude of u_{H1} in the 1:1 tuning case admits slightly higher amplitude while a substantial increase in the amplitude is observed for 2:1 tuning case. This suggests different attenuation abilities for the two tuning cases, which is further discussed in section 5.3. vi) the response of the voltage subharmonic for the 2:1 tuning validates the energy transfer and the activation of the 2:1 internal resonance. It can be realized the substantial increase in the order of magnitude of $V_{\mathrm{H1/2}}$ compared to V_{H1} of the 1:1 tuning case. v) the last major point concerns the phase angles. It appeared that in the optimal condition, the first harmonic phase angle of the displacement for both tuning cases (i.e., δ_1 and γ_2) are equal at the resonance frequency. Thus, if the first harmonic is dominant, the displacement signals corresponding to the two tuning cases will be in phase (see Fig. 20(a)). In addition, the relative phase angle γ_1, only defined for the 2:1 tuning case, admits a value of $3\pi/2$ at the antiresonance frequency, equivalent to the results obtained in [19, 20] when quadratic nonlinearities are introduced in the shunt.

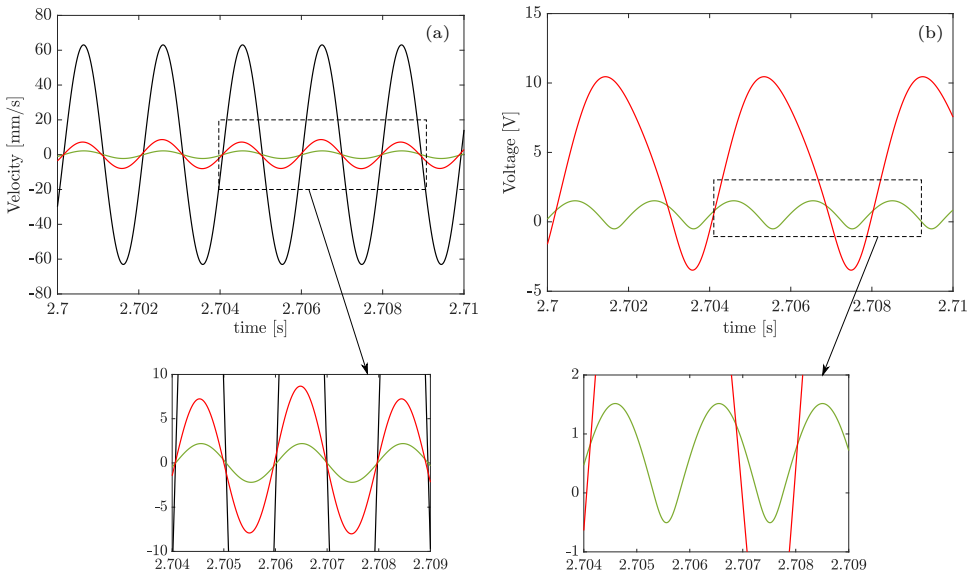

Fig. 20: (a) and (b) show respectively the measured time signals of the velocity and the PE voltage for the 1:1 tuning (in green) and 2:1 tuning (in red) at $\Omega = \hat{\omega} = 511.3 \times (2\pi)$ rad/s with excitation level $F = 5.2$ mN. For the 1:1 tuning case, we set $L = 0.73$H, $\beta = \beta^{\mathrm{op}} = 0.444$, and $R = R^{\mathrm{op}} = 237.5\Omega$. For the 1:1 tuning case, we set $L = 2.94$H,$\beta = \beta^{\mathrm{op}} = 0.4435$, and $R = R^{\mathrm{op}} = 73\Omega$.

The time signals of the velocity $v(t)$ and the PE voltage $V(t)$ are shown in Fig. 20 for the tuning cases in addition to the linear response in the open circuit configuration. The signals are recorded at the open circuit frequency (i.e., $\Omega = \hat{\omega} = 511.3 \times (2\pi)$ rad/s). The signals clearly show that for the 1:1 tuning case, the switching effect between two resonance frequencies (i.e., ω_e and ω_e' in Eq. (9)) appears clearly in PE voltage signals with a slight effect in the velocity signal. In addition, one can realize

that the velocity signals of the 1:1 tuning and 2:1 tuning in Fig. 20(a) are in phase at the resonance frequency, as suggested in Fig. 19(b). Also, one can clearly observe the presence of the subharmonic in the voltage and velocity signal in the 2:1 tuning case in Fig. 20(b), following the expressions in (42a,b).

5.2 Effect of the design parameters

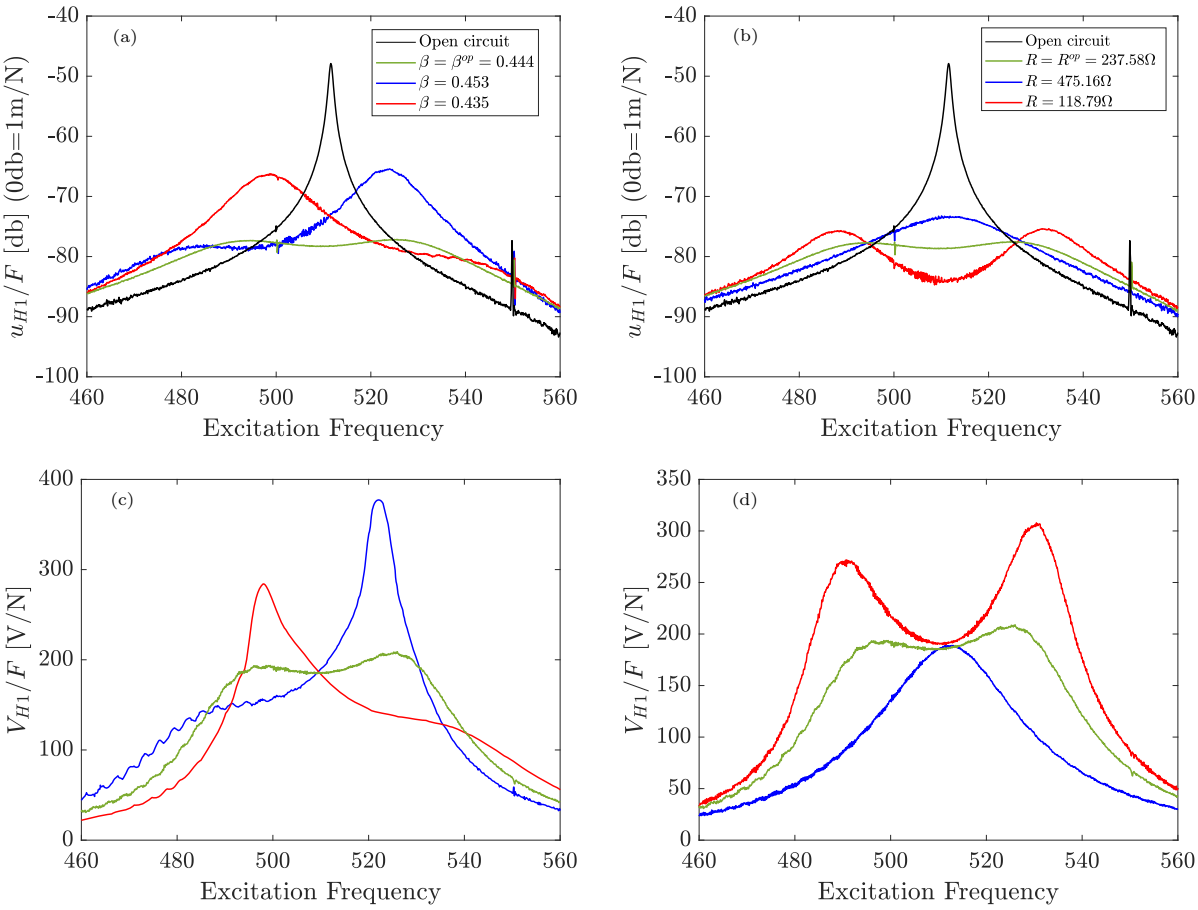

Fig. 21: Experimental frequency response of the first harmonic of the velocity u_{H1} (first row) and the PE voltage V_{H1} (second row), both normalized with respect to the excitation level, for the 1:1 tuning case. The response is shown for different values of β with $R = R^{\mathrm{op}} = 237.58\Omega$ (first column) and different values of R with $\beta = \beta^{\mathrm{op}} = 0.444$ (second column). The inductance value used in the simulations is $L = 0.737\mathrm{H} \implies r = \omega_e/\hat{\omega} = 2$. The displacement and voltage responses are plotted in dB and linear scales, respectively.

This section is devoted to show the tuning effect of the design parameters, namely the resistor in the shunt R (thus ξ_e) and the nonsmooth β. Thus, we performed two sets of experiments. In the first set, we considered three different values of β, including its optimal value, and we fixed the R at the optimum value. Similarly, in the second set, we considered three different values of R, including its optimal value, and we fixed β at its optimum value. We show in Fig. 21 the frequency responses of

u_{H1} and V_{H1} for the 1:1 tuning case and in Fig. 22, we show the frequency responses of u_{H1} and $V_{\mathrm{H1}/2}$ for the 2:1 tuning case. Regarding the value of the inductance, we consider the same setting as in Fig. 19 for both tuning cases.

One can realize from Figs. 21(a),(c) and Figs. 22(a),(c) that the response is very sensitive to β since it appears that any small perturbation of the optimal value of β in both tuning cases can break the response symmetry (i.e., the two peaks around the primary resonance admit different amplitudes) and thus shift the antiresonance from the resonance frequency. As β is varied with the resistance R_9 in the shunt circuit (see. Fig. 18), the value of this resistance should be set in a precise manner. The results in Figs. 21(b),(d) and Figs. 22(b),(d) show that setting a resistance lower than the optimal value in the shunt leads to an increase in the peaks' amplitude around the primary resonance with a decrease in the amplitude of the antiresonance. However, setting a higher value leads to the appearance of one peak near the resonance frequency in which no antiresonance is detected. The experimental results clearly validate the numerical ones in Fig. 11 and Fig. 15 for the 1:1 and 2:1 tuning cases, respectively. In addition, it is validated that the behavior with respect to β and R is equivalent to that of the linear RL-shunt but with the main difference that the tuning parameter in our case is β instead of the inductance (see Appendix A).

5.3 Discussion about the optimal attenuation

The main advantage suggested by the absorber is the ability to choose the inductance to be lower compared to that required by the RL-shunt, in which the electric resonance frequency is tuned with the nonsmooth gain β. Thus, it is necessary to experimentally validate the effect of the inductance value on the optimum attenuation suggested with the nonsmooth component. The analytical expressions of the optimal attenuation in Table 2 show that the inductance appears explicitly through the gain ϕ_1 and ϕ_2 for the 1:1 and 2:1 tuning cases, respectively. To validate those results, we measure the frequency response of u_{H1} considering the two tuning cases for different values of the inductance. The results are shown in Fig 23(a) and (b) for the 1:1 and 2:1 tuning, respectively. For each value of the inductance, we correct β and the value of R to respect the optimal condition. The 1:1 tuning suggests that the attenuation decreases as the chosen inductance in the circuit is reduced. On the contrary, the 2:1 tuning case suggests an increase of the attenuation, accompanied by a narrower bandwidth, as the inductance is reduced up to a certain level where the attenuation appears to stay constant around 22dB. Indeed, the optimal attenuation for both tuning always admits a value lower than that of the linear RL-shunt.

This attenuation behavior for both tunings is predicted through the expressions in Table. 2 as shown in Fig. 23(c) (see the solid and dashed lines). For clarity, the optimal attenuation is plotted versus the frequency ratio r instead of the inductance. Those two quantities are related by $r = \omega_e/\hat{\omega} = 1/(\hat{\omega} L C_{\mathrm{p}})$. As the results in Figs 23(a) and (b) are shown in the dB scale, the optimal attenuation, measured experimentally, is obtained by subtracting the amplitude of the linear response from that corresponding to the nonsmooth response, both measured at the resonance frequency (similar to the plots in Fig. 12 and Fig. 16). This is repeated for different values of inductance, in which the results are then plotted in Fig. 23(c) (with circle and diamond markers). Clearly, for both tunings, the experimental results follow the same pattern suggested analytically with a small discrepancy, especially for the 2:1 tuning. Realize also that we were able to reach an inductance reduction by a factor of 64 compared to that required by the linear resonant shunt with a reduction in the attenuation around 0.8dB for the 1:1 tuning case. A further reduction in the inductance was hard to be achieved in practice since it requires a value β more closer to 0.5, which can lead to unstable response.

It is worth mentioning that not only the attenuation depends on the tuning of β but indeed the whole dynamics. For example, if we consider the case with the inductance $L = 0.11$H (red curve in Fig. 23(a),(b)), the transition between the 1:1 tuning (i.e., fully linear behavior near the resonance

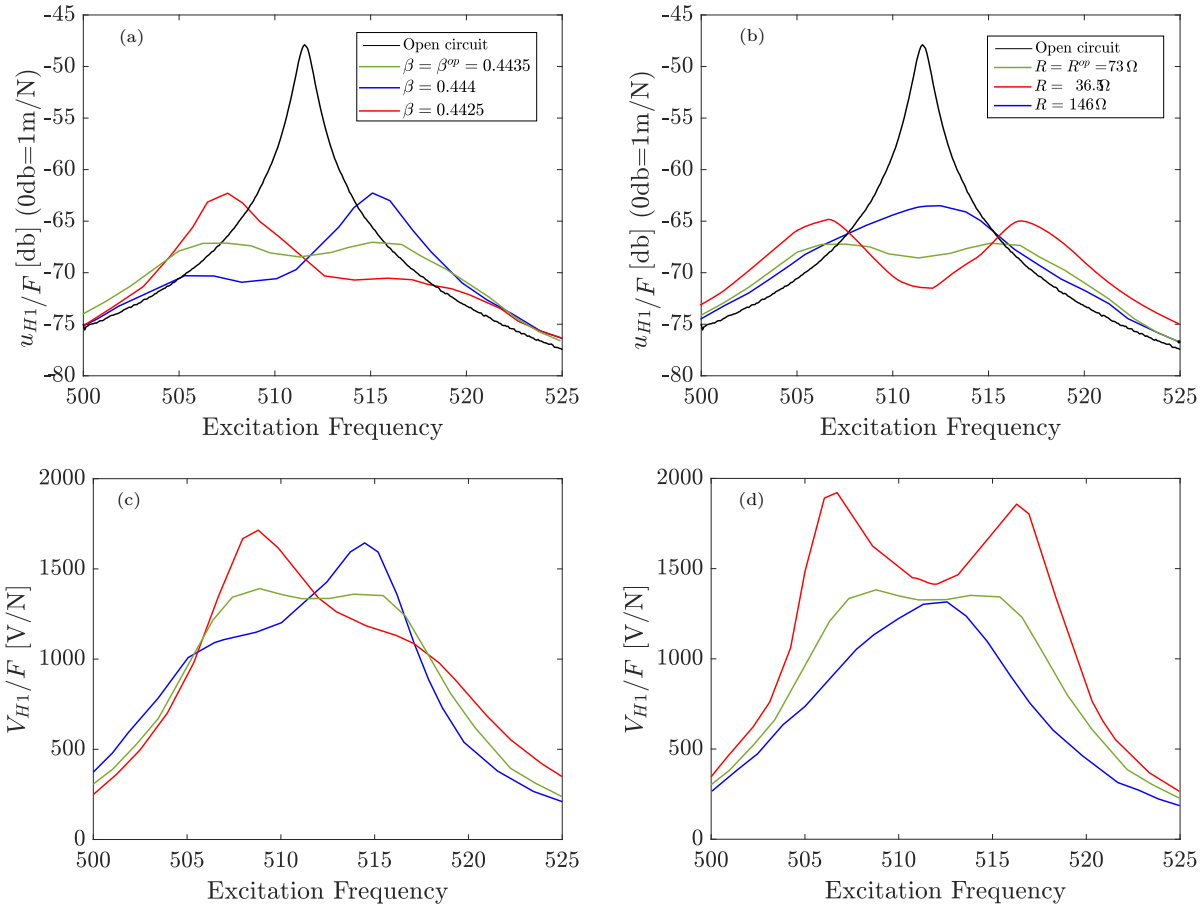

Fig. 22: Experimental frequency response of the first harmonic of the velocity u_{H1} (first row) and the PE voltage $V_{\mathrm{H1/2}}$ (second row), both normalized with respect to the excitation level, for the 2:1 tuning case. The response is shown for different values of β with $R = R^{\mathrm{op}} = 73\Omega$ (first column) and different values of R with $\beta = \beta^{\mathrm{op}} = 0.4435$ (second column). The inductance value used in the simulations is $L = 2.94\mathrm{H} \implies r = \omega_e/\hat{\omega} = 1$. The displacement and voltage responses are plotted in dB and linear scales, respectively.

frequency) to the 2:1 tuning (i.e., activation of the 2:1 internal resonance) required a change of β by around 1%. Thus, a high precision in the value of β is required to obtain the required behavior associated with each tuning case which is challenging in practice.

6 Conclusion

In this article, a new nonlinear piezoelectric shunt was proposed, based on the intentional use of a bilinear component in the electrical circuit. This nonlinear component has three important properties. The first one is to create an apparent electrical oscillation frequency $\bar{\omega}_e$ with a value that can be adjusted with the gain β, thus creating a *tunable oscillator*. The second property is that its response *is fully linear in amplitude*: despite its nonsmooth nature, no strong nonlinear behavior was observed. The nonlinearity appears through the creation of harmonics in the response of the system, mainly of

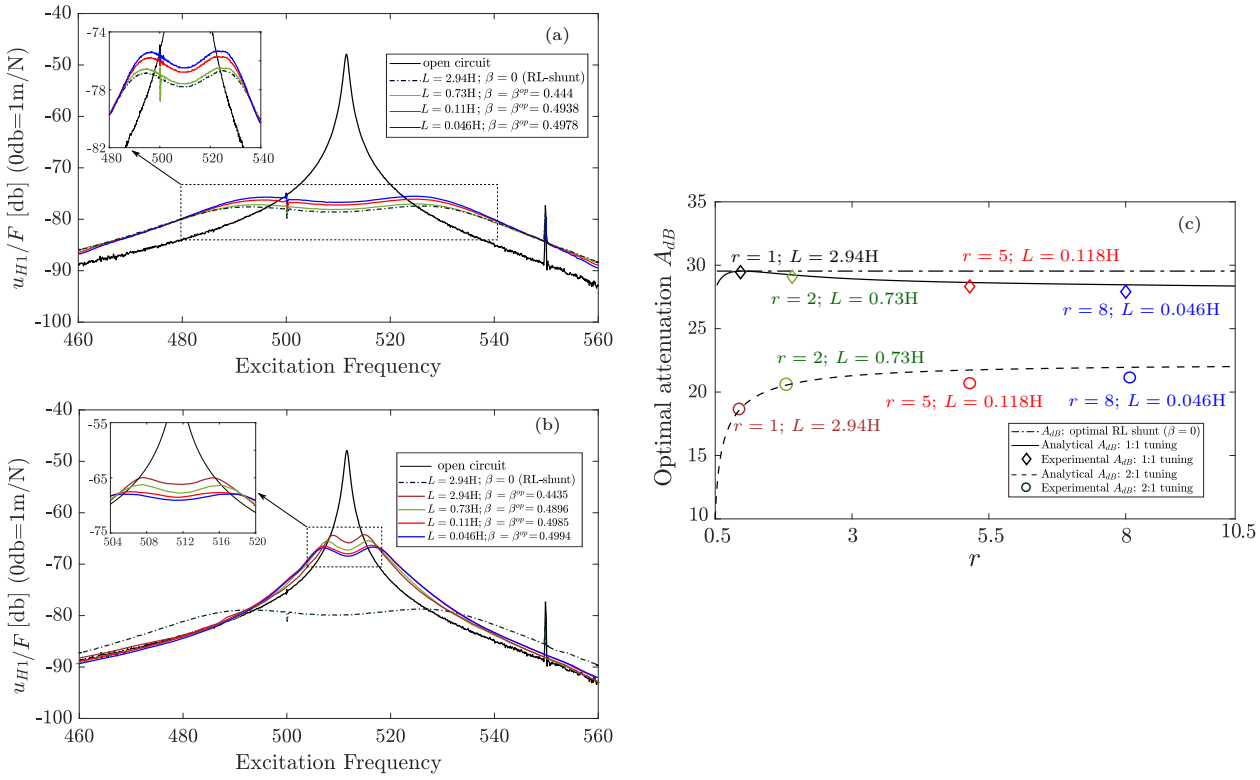

Fig. 23: (a) and (b) show the experimental frequency response of the first harmonic of the velocity u_{H1} for different values of the inductance for the 1:1 and 2:1 tuning, respectively. (c) Comparison between the optimal analytical attenuation and that measured experimentally for both tuning cases.

even order, because of its non-symmetric characteristic. The third property is that the behavior of the harmonics can be *approximated by independent linear oscillators*. Mixing those three properties, it was shown that the behavior of our shunt is (i) *equivalent to a standard RL-shunt* with (ii) the noteworthy property of being *tunable* using the gain β.

We investigated two possible tuning of the shunt. The first (classical) one is a 1:1 tuning, for which the apparent electrical frequency is tuned equal to the mechanical resonance frequency to mitigate ($\bar{\omega}_e = \hat{\omega}_i$). In this case, it was shown that it is possible to detune the RL-shunt by a factor $r_i = \omega_e/\hat{\omega}_i$ between 0.5 and 10 (in theory up to $+\infty$) without changing the amplitude reduction performance significantly: only a 1 dB decrease was observed. This tuning ability can be a considerable advantage in practice since it substantially decreases the inductance L of the shunt by a factor r_i^2, *i.e., up to a factor 100 if* $r_i = 10$.

The second tuning case, relying on a 2:1 internal resonance (the apparent electrical frequency is tuned equal to half the mechanical resonance frequency to mitigate, $\bar{\omega}_e \simeq \hat{\omega}_i/2$), shows a similar RL-shunt behavior though relying on a purely nonlinear process of energy transfer between two frequency bands, from the driving frequency Ω to its subharmonic $\Omega/2$. However, the performances are decreased since they rely on the energy transfer between the oscillators, which is weaker in the case of a 2:1 tuning with respect to the 1:1.

Even if strongly nonlinear behavior were not at hand, this nonsmooth component could pave the way for future studies involving energy harvesting and the possibility of adding quadratic and cubic

nonlinearities with the nonsmooth component in the shunt circuit to possibly obtain a response similar to an RL-shunt but associated with a saturation phenomenon. In addition, due to the multi-harmonic response generated by the nonsmooth component, and also the possible design of other nonsmooth laws for the component, the tuning cases shown in this study are not unique. One can test the possibility of other types of nonlinear modal coupling through a 1:3 internal resonance (i.e., $\bar{\omega}_e = 1/3\hat{\omega}$) or 1:2 internal resonance (i.e., $\bar{\omega}_e = 2\hat{\omega}$). The analysis of other types of internal resonance with the nonsmooth component is left for future studies.

References

1. N. Hagood and A. von Flotow, "Damping of structural vibrations with piezoelectric materials and passive electrical networks," *Journal of Sound and Vibration*, vol. 146, pp. 243–268, Apr. 1991.
2. O. Thomas, J. Ducarne, and J.-F. Deü, "Performance of piezoelectric shunts for vibration reduction," *Smart Materials and Structures*, vol. 21, p. 015008, Jan. 2012.
3. M. Berardengo, O. Thomas, C. Giraud-Audine, and S. Manzoni, "Improved resistive shunt by means of negative capacitance: new circuit, performances and multi-mode control," *Smart Materials and Structures*, vol. 25, jun 2016.
4. L. P. da Silva, W. Larbi, and J.-F. Deü, "Topology optimization of shunted piezoelectric elements for structural vibration reduction," *Journal of Intelligent Material Systems and Structures*, vol. 26, no. 10, pp. 1219–1235, 2015.
5. J.-W. Park and J.-H. Han, "Sensitivity analysis of damping performances for passive shunted piezoelectrics," *Aerospace Science and Technology*, vol. 33, no. 1, pp. 16–25, 2014.
6. A. J. Fleming, S. Behrens, and S. O. R. Moheimani, "Reducing the inductance requirements of piezoelectric shunt damping systems," *Smart Materials and Structures*, vol. 12, pp. 57–64, jan 2003.
7. B. Lossouarn, M. Aucejo, J.-F. Deü, and B. Multon, "Design of inductors with high inductance values for resonant piezoelectric damping," *Sensors and Actuators A: Physical* , vol. 259, pp. 68–76, 2017.
8. J. J. Hollkamp, "Multimodal passive vibration suppression with piezoelectric materials and resonant shunts," *Journal of intelligent material systems and structures*, vol. 5, no. 1, pp. 49–57, 1994.
9. S. Livet, M. Collet, M. Berthillier, P. Jean, and J. Cote, "Structural multi-modal damping by optimizing shunted piezoelectric transducers," *Revue Européenne de Mécanique Numérique/European Journal of Computational Mechanics*, vol. 20, no. 1-4, pp. 73–102, 2011.
10. B. Lossouarn, J.-F. Deü, and M. Aucejo, "Multimodal vibration damping of a beam with a periodic array of piezoelectric patches connected to a passive electrical network," *Smart Materials and Structures*, vol. 24, no. 11, 2015.
11. K. Marakakis, G. Tairidis, P. Koutsianitis, and G. Stavroulakis, "Shunt piezoelectric systems for noise and vibration control: A review," *Frontiers in Built Environment*, vol. 5, p. 64, 05 2019.
12. J. Gripp and D. Rade, "Vibration and noise control using shunted piezoelectric transducers: A review," *Mechanical Systems and Signal Processing*, vol. 112, p. 359, 11 2018.
13. A. F. Vakakis and O. Gendelman, "Energy Pumping in Nonlinear Mechanical Oscillators: Part II—Resonance Capture," *Journal of Applied Mechanics*, vol. 68, pp. 42–48, Jan. 2001.

14. B. Zhou, F. Thouverez, and D. Lenoir, "Essentially nonlinear piezoelectric shunt circuits applied to mistuned bladed disks," *Journal of Sound and Vibration*, vol. 333, pp. 2520–2542, Apr. 2014.

15. T. M. Silva, M. A. Clementino, C. De Marqui, and A. Erturk, "An experimentally validated piezoelectric nonlinear energy sink for wideband vibration attenuation," *Journal of Sound and Vibration*, vol. 437, pp. 68–78, Dec. 2018.

16. G. Habib, T. Detroux, R. Viguié, and G. Kerschen, "Nonlinear generalization of den hartog's equal-peak method," *Mechanical Systems and Signal Processing*, vol. 52–53, pp. 17–28, 2015.

17. P. Soltani and G. Kerschen, "The nonlinear piezoelectric tuned vibration absorber," *Smart Materials and Structures*, vol. 24, p. 075015, July 2015.

18. G. Raze, A. Jadoul, S. Guichaux, V. Broun, and G. Kerschen, "A digital nonlinear piezoelectric tuned vibration absorber," *Smart Materials and Structures*, vol. 29, p. 015007, Jan. 2020.

19. Z. A. Shami, C. Giraud-Audine, and O. Thomas, "A nonlinear piezoelectric shunt absorber with a 2:1 internal resonance: Theory," *Mechanical Systems and Signal Processing*, vol. 170, p. 108768, May 2022.

20. Z. A. Shami, C. Giraud-Audine, and O. Thomas, "A nonlinear piezoelectric shunt absorber with 2:1 internal resonance: Experimental proof of concept," *Smart Materials and Structures*, vol. 31, p. 035006, Mar. 2022.

21. Z. Shami, Y. Shen, C. Giraud-Audine, C. Touzé, and O. Thomas, "Nonlinear dynamics of coupled oscillators in 1:2 internal resonance: effects of the non-resonant quadratic terms and recovery of the saturation effect," *Meccanica*, 2022.

22. Z. A. Shami, C. Giraud-Audine, and O. Thomas, "Antiresonance detuning correction for a piezoelectric shunt absorber based on 2:1 internal resonance using a cubic nonlinearity," *Smart Materials and Structures*. Under review.

23. C. Touzé, O. Thomas, and A. Chaigne, "Asymmetric non-linear forced vibrations of free-edge circular plates. part 1: Theory," *Journal of Sound and Vibration*, vol. 258, pp. 649–676, Dec. 2002.

24. A. Givois, A. Grolet, O. Thomas, and J.-F. Deü, "On the frequency response computation of geometrically nonlinear flat structures using reduced-order finite element models," *Nonlinear Dynamics*, vol. 97, pp. 1747–1781, July 2019.

25. A. H. Nayfeh, *Perturbation Methods*. Wiley Classics Library, New York: John Wiley & Sons, wiley classics library ed., 2000.

26. I. Kovacic, L. Cveticanin, M. Zukovic, and Z. Rakaric, "Jacobi elliptic functions: A review of nonlinear oscillatory application problems," *Journal of Sound and Vibration*, vol. 380, pp. 1–36, Oct. 2016.

27. C. Touzé, "Normal form theory and nonlinear normal modes: Theoretical settings and applications," in *Modal Analysis of Nonlinear Mechanical Systems* (G. Kerschen, ed.), vol. 555, pp. 75–160, Vienna: Springer Vienna, 2014.

28. A. Darabi and M. J. Leamy, "Clearance-type nonlinear energy sinks for enhancing performance in electroacoustic wave energy harvesting," *Nonlinear Dynamics*, vol. 87, pp. 2127–2146, Mar. 2017.

29. Y. S. Lee, F. Nucera, A. F. Vakakis, D. M. McFarland, and L. A. Bergman, "Periodic orbits, damped transitions and targeted energy transfers in oscillators with vibro-impact attachments," *Physica D: Nonlinear Phenomena*, vol. 238, pp. 1868–1896, Sept. 2009.

30. M. Vakilinejad, A. Grolet, and O. Thomas, "A comparison of robustness and performance of linear and nonlinear lanchester dampers," *Nonlinear dynamics*, vol. 100, pp. 269–287, 2020.

31. S. Benacchio, C. Giraud-Audine, and O. Thomas, "Effect of dry friction on a parametric nonlinear oscillator," *Nonlinear Dynamics*, vol. 108, pp. 1005–1026, Apr. 2022.

32. F. Georgiadis, A. F. Vakakis, D. M. McFarland, and L. Bergman, "Shock Isolation Through Passive Energy Pumping in a System With Piecewise Linear Stiffnesses," in *Volume 5: 19th Biennial Conference on Mechanical Vibration and Noise, Parts A, B, and C*, (Chicago, Illinois, USA), pp. 1569–1574, ASMEDC, Jan. 2003.

33. C.-H. Lamarque, O. V. Gendelman, A. Ture Savadkoohi, and E. Etcheverria, "Targeted energy transfer in mechanical systems by means of non-smooth nonlinear energy sink," *Acta Mechanica*, vol. 221, pp. 175–200, Sept. 2011.

34. C.-H. Lamarque, A. Ture Savadkoohi, and Z. Dimitrijevic, "Dynamics of a linear system with time-dependent mass and a coupled light mass with non-smooth potential," *Meccanica*, vol. 49, pp. 135–145, Jan. 2014.

35. B. Youssef and R. I. Leine, "A complete set of design rules for a vibro-impact NES based on a multiple scales approximation of a nonlinear mode," *Journal of Sound and Vibration*, vol. 501, p. 116043, June 2021.

36. X.-F. Geng and H. Ding, "Theoretical and experimental study of an enhanced nonlinear energy sink," *Nonlinear Dynamics*, vol. 104, pp. 3269–3291, June 2021.

37. C. Richard, D. Guyomar, D. Audigier, and G. Ching, "Semi-passive damping using continuous switching of a piezoelectric device," in *SPIE Smart Structures and Materials Conference*, vol. 3672, pp. 104–111, 1999.

38. J. Ducarne, O. Thomas, and J.-F. Deü, "Structural Vibration Reduction by Switch Shunting of Piezoelectric Elements: Modeling and Optimization," *Journal of Intelligent Material Systems and Structures*, vol. 21, pp. 797–816, 2010.

39. C. Richard, D. Guyomar, D. Audigier, and H. Bassaler, "Enhanced Semi-passive Damping Using Continuous Switching of a Piezoelectric Device on an Inductor," in *Proceedings of SPIE Smart Structures and Materials Conference: Passive Damping and Isolation*, vol. 3989, pp. 288–299, 2000.

40. L. Petit, E. Lefeuvre, C. Richard, and D. Guyomar, "A Broadband Semi Passive Piezoelectric Technique for Structural Damping," in *Proceedings of SPIE Smart Structures and Materials Conference: Passive Damping and Isolation*, vol. 5386, pp. 414–425, 2004.

41. E. Lefeuvre, A. Badel, L. Petit, C. Richard, and D. Guyomar, "Semi-passive Piezoelectric Structural Damping by Synchronized Switching on Voltage Sources," *Journal of Intelligent Material Systems and Structures*, vol. 17, pp. 653–660, 2006.

42. A. Badel, G. Sebald, D. Guyomar, M. Lallart, E. Lefeuvre, C. Richard, and J. Qiu, "Piezoelectric vibration control by synchronized switching on adaptive voltage sources: Towards wideband semi-active damping," *The Journal of the Acoustical Society of America*, vol. 119, pp. 2815–2825, 2006.

43. J. Ducarne, O. Thomas, and J. Deü, "Vibration reduction by switch shunting of piezoelectric elements: nonlinear energy transfers between modes and optimization," in *Proc. of the 19th. International Conference on Adaptative Structures and Technologies*, (Ascona, Switzerland), Oct. 2008.

44. L. Guillot, B. Cochelin, and C. Vergez, "A taylor series-based continuation method for solutions of dynamical systems," *Nonlinear Dynamics*, vol. 98, pp. 2827–2845, 2019.

45. L. Guillot, A. Lazarus, O. Thomas, C. Vergez, and B. Cochelin, "A purely frequency based floquet-hill formulation for the efficient stability computation of periodic solutions of ordinary differential systems," *Journal of Computational Physics*, vol. 416, p. 109477, 2020.

46. L. Pernod, B. Lossouarn, J.-A. Astolfi, and J.-F. Deü, "Vibration damping of marine lifting surfaces with resonant piezoelectric shunts," *Journal of Sound and Vibration*, vol. 496, p. 115921, 2021.

47. O. Thomas, C. Touzé, and A. Chaigne, "Asymmetric non-linear forced vibrations of free-edge circular plates, part 2: experiments," *Journal of Sound and Vibration*, vol. 265, no. 5, pp. 1075–1101, 2003.

48. M. Vatavu, V. Nastasescu, F. Turcu, and I. Burda, "Voltage-controlled synthetic inductors for resonant piezoelectric shunt damping: A comparative analysis," *Applied Sciences*, vol. 9, no. 22, 2019.

Statements & Declarations

The authors declare that they have no known competing financial interests or personal relationships that could have appeared to influence the work reported in this paper.
The Région Hauts de France and the Carnot ARTS Institute, France are warmly thanked for the PhD grant of the first author.

Data Availability

The datasets generated during and/or analysed during the current study are not publicly available but are available from the corresponding author on reasonable request.

Appendix A: RL-shunt response and optimization: reference solution

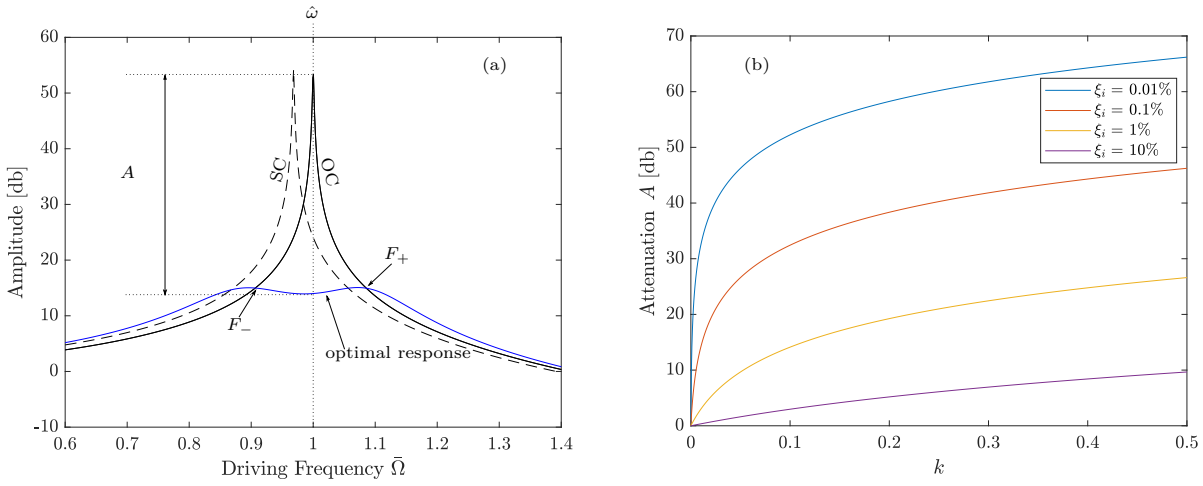

Fig. 24: (a) Typical FRF of the RL-shunt in the optimal case. (b) Attenuation A as function of k for different mechanical damping factor ξ_i.

In this section, we recall the response of a mechanical system coupled to a RL-shunt. We thus consider Eqs. (21a,b) without the nonsmooth term (i.e., $\beta = 0 \Rightarrow \bar{r}_i = r_i, \bar{k}_i = k_i$), which reads:

$$\ddot{\tilde{q}}_i + 2\xi_i \dot{\tilde{q}}_i + \tilde{q}_i + k_i r_i \tilde{Q} = f_i \cos \tilde{\Omega} \tilde{t}, \tag{A.1a}$$

$$\ddot{\tilde{Q}} + 2\xi_e r_i \dot{\tilde{Q}} + r_i^2 \tilde{Q} + k_i r_i \tilde{q}_i = 0. \tag{A.1b}$$

The mechanical FRF is thus:

$$H_q(\tilde{\Omega}) = \hat{\omega}_i^2 m_i \frac{\mathring{q}}{F} = \frac{r_i^2 - \tilde{\Omega}^2 + 2j\tilde{\Omega}\xi_e r_i}{\left(1 - \tilde{\Omega}^2 + 2j\tilde{\Omega}\xi_i\right)\left(r_i^2 - \tilde{\Omega}^2 + 2j\tilde{\Omega}\xi_e r_i\right) - k_i^2 r_i^2}, \tag{A.2}$$

where $\mathring{q}_i(\tilde{\Omega})$ is the Fourier transform of $q_i(t)$.

As a classical result (see e.g., [2]), it is possible to choose the electrical frequency ω_e and the damping ratio ξ_e such that the amplitude of the i-th resonance of the elastic structure is minimized and has a blunt shape, shown in Fig. 24(a). The optimal values of ω_e and ξ_e are:

$$\omega_e^{\text{op}} = \hat{\omega}_i \quad \Rightarrow \quad r_i^{\text{op}} = 1; \quad \xi_e^{\text{op}} = \frac{\sqrt{6} k_i}{4}. \tag{A.3}$$

Then, as in [2], a performance indicator of the RL-shunt can be defined as the difference, in dB, between the amplitude at the resonance of the mechanical oscillator without shunt (for instance, with the shunt in open-circuit) and the maximum amplitude of the blunt shunt with the optimal RL-shunt. Here, to simplify, we define the latter as the amplitude at the open circuit frequency, i.e., for $\Omega = \hat{\omega}_i$ ($\tilde{\Omega} = 1$). The optimal attenuation A_{dB} is then estimated with Eq. (A.2) as:

$$A_{\text{dB}} = 20 \log_{10} \frac{H_q|_{k_i=0}(\tilde{\Omega} = 1)}{H_q|_{\xi_e = \xi_e^{\text{op}}, r_i = 1}(\tilde{\Omega} = 1)} = 20 \log_{10} \left(1 + \frac{k_i}{\xi_i \sqrt{6}}\right) \tag{A.4}$$

Eq. (A.4) suggests that the attenuation is solely function of the mechanical damping factor ξ_i and the piezoelectric coupling k_i, as shown in Fig. 24(b). Note that the above expression for A_{dB} is taken at the open circuit frequency and not at the frequency of the fixed points as in [2] to obtain a simpler expression whose numerical value is very close.

Appendix B: Regularization of the nonsmooth term and implementation in MANLAB

The numerical results in this work were all obtained using Manlab, which requires regularization of the nonsmooth term associated with the absolute value function of the piezoelectric voltage $|V|$. As a first step, we define a new variable y as:

$$y = |V| \quad \Longrightarrow \quad \begin{cases} y = -V & \text{if} \quad V < 0, \\ y = V & \text{if} \quad V > 0. \end{cases} \tag{B.1}$$

Then, the regularization is obtained through the following equation:

$$(y - V)(y + V) = \delta \quad \Longrightarrow \quad y^2 - V^2 - \delta = 0, \tag{B.2}$$

where $\delta \in \mathbb{R}$ is the regularization parameter. As seen in Fig. 25, if $\delta = 0$, the solution is equivalent to $y = |V|$. For a small value of δ, the angular point at $V = 0$ of the graph of the absolute value function is replaced by a smooth curve that gets closer to the nonsmooth exact one as δ approaches zero.

Upon obtaining the regularization, the two degree of freedom system in (2a,b) is implemented in MANLAB in the first order form considering four main variables (q, Q, v, w) and two auxiliary variables (V, y) [45]:

$$\begin{cases} \dot{q}_i = v, & \text{(B.3a)} \\ \dot{Q} = w, & \text{(B.3b)} \\ \dot{v} = -2\xi_i \hat{\omega}_i v - \hat{\omega}_i^2 q_i - \dfrac{\theta_i}{m_i C_{\text{p}i}} Q + \dfrac{F}{m_i} \cos \Omega t, & \text{(B.3c)} \\ \dot{w} = -2\xi_e \omega_e w - \omega_e^2 Q - \dfrac{\theta_i}{L C_{\text{p}i}} q_i - \dfrac{\beta}{L} (y + V), & \text{(B.3d)} \\ 0 = V - \dfrac{1}{C_{\text{p}i}} (Q + \theta_i q_i), & \text{(B.3e)} \\ 0 = y^2 - V^2 - \delta, & \text{(B.3f)} \end{cases}$$

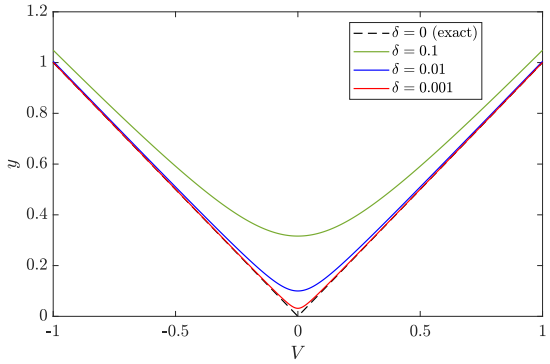

Fig. 25: Graph of the function $y = |V|$ and its regularized versions for different values of δ.

where Eqs. (B.3a,b,c,d) are the main equations and Eqs. (B.3e,f) are the auxiliary equations introduced to obtain the voltage V and the regularization variable y.

Appendix C: Tuning ratio for the 2:1 tuning

Following the reasoning used in [19], we consider the linear system (21a, b). Since the stiffness part is not diagonal, it is possible to compute its two dimensionless frequencies, which read:

$$\omega_1^2 = \frac{1 + \bar{r}_i^2 - \sqrt{\Delta}}{2}, \quad \omega_2^2 = \frac{1 + \bar{r}_i^2 + \sqrt{\Delta}}{2}, \tag{B.4}$$

with $\Delta = (1 - \bar{r}_i^2)^2 + 4\bar{k}_i^2\bar{r}_i^2$. Enforcing $\omega_2 = 2\omega_1$, one arrives to the following order 2 polynomial in $\bar{r}_i^2$:

$$4\bar{r}_i^4 + (25\bar{k}_i^2 - 17)\bar{r}_i^2 + 4 = 0, \tag{B.5}$$

that have two roots. r_i^* of Eq. (33) is the one which is smaller than 1, close to 0.5.